Bioprinting 20 (2020) e00108

Contents lists available at ScienceDirect

Bioprinting

journal homepage: www.elsevier.com/locate/bprint

Research paper

Microfluidic bioprinting towards a renal *in vitro* model

Gabriele Addario [a,1], Sonja Djudjaj [b,1], Silvia Farè [c], Peter Boor [b,d,e], Lorenzo Moroni [a], Carlos Mota [a,*]

[a] Maastricht University, MERLN Institute for Technology-Inspired Regenerative Medicine, Complex Tissue Regeneration Department, 6229 ER, Maastricht, the Netherlands
[b] Institute of Pathology, RWTH University of Aachen, Aachen, Germany
[c] Dipartimento di Chimica, Materiali e Ingegneria Chimica, Politecnico di Milano, Milano, Italy
[d] Division of Nephrology, RWTH University of Aachen, Aachen, Germany
[e] Electron Microscopy Facility, RWTH University of Aachen, Aachen, Germany

ARTICLE INFO

Keywords:
Microfluidic
Bioprinting
Core-shell
Kidney
Renal 3D models
Polysaccharides

ABSTRACT

It is estimated that 10% of the worldwide population suffers from chronic kidney disease (CKD) with a rising tendency. Patients with CKD have limited treatment options and novel therapies that could halt or even reverse the progression of CKD are urgently needed.

Bioprinting is considered one of the most promising approaches to generate novel 3D *in vitro* models and organ-like constructs to investigate underlying pathomechanism of kidney diseases. This study aimed at establishing a method to isolate primary renal cells in an easy and reproducible way. These cells were used in a new bioprinting platform laying the foundation for the development of a 3D renal tubulointerstitium model for *in vitro* studies. Primary murine tubular (pmTECs), endothelial and fibroblast cells were successfully isolated, but further optimization is required for the culture and expansion of primary endothelial cells. Therefore, an endothelial cell line (HUVECs) and pmTECs were combined with polysaccharide biomaterial ink solutions and processed with a microfluidic 3D bioprinter, leading to high cell viability and metabolic activity. Core-shell bioprinted constructs with HUVECs and pmTECs were manufactured mimicking tubules.

In conclusion, microfluidic bioprinting strategy could be used to build a novel 3D kidney *in vitro* model.

1. Introduction

It is estimated that 10% of the worldwide population suffers from CKD [1]. Among these, 10–20% of the patients experience a progressive loss of renal function, leading to end-stage renal disease (ESRD) [1,2]. ESRD patients undergo life-saving renal replacement therapies such as haemodialysis and peritoneal dialysis, while waiting for a suitable donor organ. Kidney transplantation is the ultimate therapy but the low availability of matching donor organs limits this approach. Furthermore, after transplantation there is still a high risk of organ rejection, cardiovascular complications and cancer, the latter one enhanced by the use of immunosuppression [3]. Because of the limitations in current conventional therapies, it is of utmost importance to develop new strategies to study *in vitro* the renal disease progression [1].

Kidney fibrosis is considered the best predictor of progression and irreversibility of CKD [4,5]. Fibrosis is the pathological endpoint of CKD, in which activated mesenchymal cells replace the functional parenchyma and an excessive accumulation of extracellular matrix (ECM) is normally observed. The underlying mechanism of this cascade of events is still not clear [4,5]. It has been shown that fibrosis is triggered by an orchestrated cross-talk of a multitude of cell types, in particular epithelial, endothelial, immune cells and mesenchymal cells such as fibroblasts [6]. Tubular epithelial cells (TECs) make up the majority of renal parenchyma and react sensitively to a wide range of stress stimuli. TECs have a high regenerative capacity and mild tubular injuries are normally repaired. However, severe or repetitive injuries lead to permanent damage up to tubular atrophy and is associated with renal fibrosis. Tubular injury leads to an activation and increase of fibroblasts, the resident mesenchymal cells in the renal tubulointerstitium. Several mechanisms for the increase of these activated fibroblasts, so called myofibroblasts, are described in the literature. The major proposed mechanisms for the myofibroblast increase is the proliferation of resident fibroblasts [7]. Other sources for

* Corresponding author.
E-mail addresses: g.addario@maastrichtuniversity.nl (G. Addario), sdjudjaj@ukaachen.de (S. Djudjaj), silvia.fare@polimi.it (S. Farè), pboor@ukaachen.de (P. Boor), l.moroni@maastrichtuniversity.nl (L. Moroni), c.mota@maastrichtuniversity.nl (C. Mota).
[1] these authors contribute equally to the study.

https://doi.org/10.1016/j.bprint.2020.e00108
Received 14 July 2020; Received in revised form 23 September 2020; Accepted 7 October 2020

myofibroblasts are described, such as the transformation from tubular epithelial cells to mesenchymal cells, known as epithelial-to-mesenchymal transition (EMT) [8,9]. Further sources of myofibroblasts have been associated to endothelial cells of peritubular capillaries undergoing endothelial-to-mesenchymal-transition (EndMT) and circulating fibrocytes [6]. Due to this complex interplay of different cell types, animal models are currently the only option to investigate the development of kidney diseases and the progression to renal fibrosis [3].

Alternatives to animal models reflecting the complex cellular structures of the kidneys are required, but currently missing. Compared to traditional 2D cell culture, 3D models can mimic more closely the renal physiology. Generally, in 3D models the cell morphology, polarization, expression of key transporters and the metabolic activity is more preserved, and the expression of cell injury markers is normally reduced [10,11]. Currently, *in vitro* 3D culture models of kidney compartments are under investigation. The simplest method is the co-culture of different cell types in a 3D casted hydrogel. A recent example of such 3D culture approach was used to combine human renal proximal tubular cells and fibroblasts with a collagen type I hydrogel to confirm the hypothesis of EMT in fibrosis [12]. Human dermal fibroblasts were used in this model instead of renal fibroblasts, which would be more relevant to investigate kidney fibrosis. Additionally, this model lacked other cell types, e.g. leukocytes or macrophages that play an important role in the development of renal fibrosis. Another recently developed method relies on kidney organoids, which are capable of spontaneously organise into structures resembling nephron rudiments. These nephrons are not fully differentiated and they lack a vital vasculature [3]. The third option is bioprinting, considered one of the most promising techniques to create renal 3D *in vitro* models. Biomaterial inks and cells are combined to form bioink formulations and these are selectively dispensed in a predesigned architecture [13]. Bioprinting enables a gradual build-up of complex structures as found in the kidney. Some initial literature reports aimed at the bioprinting of renal tubular models but, in most cases, no cells were included in the process, thus the full potential of bioprinting is yet to be demonstrated [11,14,15]. Only recently, a reported study used core-shell bioprinting strategies to manufacture tubular constructs containing cells to create endothelial and epithelial tubular compartments [16]. In addition, the screening and testing of different cell types from different origin and biomaterial inks to produce such bioprinted renal *in vitro* model is largely missing.

The aim of this study was to establish a robust protocol for the isolation of primary murine kidney cells and to test their suitability for bioprinting. As tubular epithelial cells are the major cell type in the kidney, we aimed to start with these cells and used for isolation a transgenic K8-YFP reporter mouse. We established a method to isolate primary murine tubular epithelial cells (pmTECs), fibroblast and endothelial cells (ECs), but further culturing was only successful for pmTECs and fibroblasts. Therefore, we used an endothelial cell line (HUVECs) for further bioprinting experiments, implementing a new microfluidic bioprinting platform. The processing parameters to bioprint polysaccharide-based biomaterial inks were optimized. We tested our optimized bioprinting protocol with bioinks containing pmTECs and HUVECs, investigating cell survival and metabolic activity of the bioprinted constructs. Bioinks were processed in a core-shell arrangement to mimic the tubulointerstitium, where the peritubular capillaries wrap the renal tubule. In summary, the primary isolated cells are suitable for the improved microfluidic bioprinting process offering future possibility to investigate cell behaviour within the bioprinted constructs without the need for further stainings. This study lays the basis for an alternative 3D *in vitro* model for the investigation of mechanisms, potential therapies and the development of renal fibrosis.

2. Materials and methods

2.1. Healthy and disease animal models

Animals were housed under standard conditions in a light, temperature- and humidity-controlled environment with free access to tap water and standard rodent chow. All animal protocols were approved by the local government authorities (Landesamt für Umwelt und Verbraucherschutz Nordrhein Westfalen AZ 84-02.04.2014.A518). Transgenic K8-YFP (n = 3) (kindly provided by the research group of Prof. Rudolf Leube and Dr. Nicole Schwarz, RWTH Aachen University, Aachen, Germany) and wildtype mice (n = 3) underwent unilateral ureter obstruction (UUO) and were sacrificed after 5 days. Upon sacrifice, both healthy contralateral and UUO kidneys were harvested. 5/6 of the kidneys were used to isolate primary cells, the rest of the kidney was fixed for 4 h in 3% PFA, equilibrated in 30% sucrose overnight and stored in TissueTek for cryosections.

2.2. Cell isolation and culture

Primary murine tubular epithelial cells (pmTEC), endothelial cells and fibroblasts were isolated from K8-YFP transgenic mice as shown in Figure S1. In short, kidney were removed and kept in Dulbecco's Modified Eagle Medium/Ham's F-12 (Gibco, DMEM/F-12) supplemented with 1% penicillin and 1% streptomycin. After encapsulation, kidneys were digested for 30 min at 37 °C in Collagenase IV (1 mg/ml). Digestion was stopped with the addition of 0.1% fetal calf serum (FCS) and sieved to remove large vessels and tissue pieces. After washing in PBS, cells were seeded in cell-specific media for selective cell growth or further processed for FACS sorting.

PmTECs were cultured in advanced Dulbecco's Modified Eagle Medium/Ham's F-12 (Gibco, DMEM/F-12) supplemented with 0.1 µg/ml reconstituted mouse recombinant epidermal growth factor (Gibco, rEGF), 0.2% v/v hydrocortisone (Sigma-Aldrich, H6909), 1.4% v/v 4-(2-hydroxyethyl)-1-piperazineethanesulfonic acid buffer solution (Gibco, HEPES) and 1% v/v L-Glutamine (Gibco). Cells were cultured in T25 cell culture flasks (Thermo Scientific) coated with a mixture of a 0.02% v/v gelatin solution (Sigma-Aldrich, type B, prepared in ultrapure water) and fibronectin (5 µg/ml) from bovine plasma (Sigma-Aldrich). Coating was performed by incubating the mixture for 1 h at 37 °C with subsequent removal of the liquid.

Primary fibroblasts were cultured in DMEM high glucose with 10% v/v FCS. Primary endothelial cells and human umbilical vein endothelial cells (HUVEC, EGM-2, cryo amp, from Lonza, catalog #C2519A) were cultured in endothelial cell growth medium 2 (EGM-2, bio-connect C-22011). All cell types were cultured in an incubator at 37 °C, 5% CO_2.

2.3. Fluorescence activated cell sorting (FACS)

Flow cytometry of single cell suspension, freshly isolated from the tissue, was prepared as described under cell isolation. After filtering the digest with a 70 µm cell strainer, cell suspension was transferred to a 50 ml syringe and pushed through a 27 Gauge needle 3 to 5 times. Finally, single cell suspension was spilled through 40 µm cell strainer and divided in lots. For detection of the endogenous signal of K8-YFP of the pmTECs, the cell suspension was left untreated. For sorting of endothelial cells, cells were stained with CD31-PE (BD Bioscience). Flow cytometry was performed on a BD FACSAria II ™ and on a BD FACSCalibur™ (BD Biosciences, Heidelberg, Germany). Whole procedure was performed with minimal exposure to light to prevent alterations to the fluorescent signal.

2.4. Immunofluorescence and immunocytochemistry

Frozen renal tissue was cut into 5-µm sections and mounted on a glass slide. After 30 min of drying at room temperature, the tissue was hydrated with PBS and counterstained with DAPI. Finally, samples were mounted with Immu-Mount™ (Thermo Scientific, Rockford, USA). For immunocytochemical analysis, cells cultured on cover slips pre-coated with 2 µg/cm^2 collagen IV in 24-well plates were stained as previously described [17].

2.5. Biomaterial ink preparation

Different biomaterial inks were used: a commercially available alginate solution (AG-10™ Matrix, Aspect Biosystems, Canada) hereafter defined as C_alginate, an in-house alginate solution (Sigma-Aldrich, alginic acid sodium salt from brown algae, low viscosity) hereafter defined as IH_alginate, a gelatin solution (Sigma-Aldrich, gelatin from bovine skin, type B) and a pectin solution (Herbstreith & FOX, Germany). C_alginate solution was provided ready to use, autoclaved, and prepared in a milliQ water-based saline solution. IH_alginate solution and the gelatin solution were prepared in Dulbecco's phosphate buffered saline (PBS, without calcium chloride and magnesium chloride, sterile) on a stirring plate at room temperature until a homogenous solution was obtained. The pectin solution was produced following a protocol by Neves et al. [18]. Briefly, 1 wt% pectin solution was prepared in 0.1 M 2-(N-morpholino) ethanesulfonic acid (MES, Sigma-Aldrich) buffer solution (0.1 M MES, 0.3 M NaCl buffer) in milliQ water, with the pH adjusted to 6, using 1 M NaOH (Sigma-Aldrich). Purification was performed using 2 wt% activated charcoal (Sigma-Aldrich), followed by centrifugation, filtration and lyophilization. The pectin biomaterial ink solution was prepared by dissolving the lyophilized pectin in 0.9 wt% NaCl in milliQ water on a stirring plate, at room temperature, until a homogenous solution was obtained. The prepared biomaterial ink solutions were sterile filtered using a 0.22 μm filter. A $CaCl_2$-based crosslinker solution (CAT-2™ crosslinker, Aspect Biosystems, Canada) and a saline buffer solution (Aspect Biosystems, Canada) were used as received, if not differently indicated.

2.6. Material characterization

IH_alginate and pectin solutions were characterized in terms of dynamic viscosity using an Ubbelohde viscometer (SI Analytics, type no. 530 20). For the pectin biomaterial ink, a study on the effect of the solution pH on the viscosity was performed [19–23]. A comparison between the pectin without pH correction (pH = 3.54) and with the pH correction (pH = 6) was performed. The pH was measured using a pH meter (Mettler Toledo-FiveEasy Plus). All the measurements (n = 3) were done at room temperature (21.5 °C).

In addition, the molecular weight of C_alginate and IH_alginate was measured by means of liquid chromatography (Shimadzu Prominence LC equipped with RU and PDA detectors), setting the temperature to 25 °C and the pressure to 34 bar. Samples were prepared dissolving 1 mg of lyophilized alginate in 1 ml of 0.1 M $NaNO_3$.

2.7. Parametric study of processing parameters and manufacturing of 3D structures

A commercial microfluidic bioprinter (RX1 Aspect Biosystems, Canada) was used (Fig. 2a). The bioprinter main dispensing technology is based on microfluidic principles, with a disposable printhead. A dual biomaterial printhead (DUO printhead, Aspect Biosystems, Canada) designed to process up to two materials enables an accurate combination of multiple flow streams of the two biomaterial inks or bioinks and crosslinker or buffer solutions (Fig. 2a). Air pressure is the driving force that controls the opening/closure of the valves of the printhead and the pressurization of the reservoirs containing the individual solutions. The combination of biomaterial inks or bioinks with the crosslinker triggers a fast ionic physical gelation, forming a filament before leaving the nozzle of the printhead. Furthermore, the crosslinker involves the filament acting as a shielding fluid minimizing the shear stress on the encapsulated cells.

The bioprinting process parameters, i.e. crosslinker pressure, material pressure, translation velocity, and offset (distance between the nozzle and the cell culture plate inserts) were investigated for the alginate (C_alginate and IH_alginate) and pectin biomaterial inks solutions. The influence of these parameters on the bioprinted construct was studied by varying one individual parameter and keeping the remaining ones constant. We investigated how a single process variable can influence the diameter of the bioprinted filament and the stability. For this purpose, a rectangular volume with 0.2 × 0.2 × 40 mm was created on the bioprinter's software and the deposition pattern was generated to allow the manufacturing of single filaments with 40 mm length. The influence of the different process parameters on the filament diameter was evaluated on samples (n = 3) manufactured for the different combinations of the process parameters. The bioprinted filaments were washed with PBS and analysed under the microscope (Nikon Eclipse Ts2 Inverted Microscope). The filament diameter was measured in multiple regions (n = 4) by analysing the acquired images with ImageJ 1.52 K software. When the optimal bioprinting parameters in terms of deposition and the filament diameter of approximately 200 μm were obtained, the manufacturing of 3D structures was investigated. Structures such as hollow cylinders (6 mm height, external diameter of 15 mm, internal diameter of 14.8 mm) and cubes (6 × 6 × 6 mm^3) were manufactured. These structures were bioprinted in cell culture plate inserts (ThinCert™, Greiner Bio-one) with a pore size of 8 μm, allowing the removal of the crosslinker and buffer solution excess. The 3D bioprinted structure was imaged using a stereomicroscope (Nikon, smz 25).

2.8. Bioprinting and cell viability assay

The previously described bioprinter allows the design of multiple deposition strategies by dispensing precisely individual or simultaneously the bioinks during the biofabrication of the 3D constructs. The system was installed in a class II biosafety laminar flow cabinet to ensure the sterility necessary for the bioprinting process while maintaining the operator safe. In this study, pmTECs and HUVECs were used and individually combined with the biomaterial inks with a cell density of 2 × 10^6 cells/ml [15]. The centrifuged cell pellet was pipetted into the biomaterial ink solution and mixed thoroughly to ensure uniform dispersion of the cells. Cubic structures were extruded on the cell culture plate inserts, undergoing a post-crosslinking for 5 min, by immersing the constructs in a sterile filtered 125 mM $CaCl_2$ solution prepared in milliQ water. Each bioprinted condition was conducted alongside with the production of 20 μl droplets, i.e. manually micropipetted bioinks, which were used as a control to test the influence of the bioprinting process on the cell viability. The droplets were crosslinked using the commercial crosslinker, followed by the same post-crosslinking procedure performed to the bioprinted structures. A cell viability assay was performed on the bioprinted constructs and droplets. The live/dead staining was performed using three fluorescent dyes: calcein blue AM (ex/em 322/435 nm), calcein green AM (ex/em 495 nm/515 nm) and ethidium homodimer (EthD-1) (ex/em 495 nm/635 nm), from ThermoFisher Scientific. Calcein AM is a cell-permeant dye that marks enzymatic active and membrane intact cells, being retained in viable cells, emitting an intensive green/blue fluorescence signal. EthD-1 is impermeable in viable cells and its affinity to bound to DNA expresses a high red fluorescence signal. Live/dead assay was performed on day 1, 3 and 7. Hanks' balanced salt solution (HBSS, modified, with calcium, with magnesium, Sigma-Aldrich) was used to dilute the stock solutions of the dyes produced following the supplier recommendations. Live/dead images were acquired using a live cell microscope (Nikon eclipse Ti, Japan) equipped with a Zyla camera and an OXO incubator to keep the samples at 37 °C, 5% CO_2 during the image acquisition. The obtained images were processed using NIS software (Nikon) and ImageJ 1.52 K software.

2.9. Metabolic activity

A resazurin-based cell metabolic activity assay (PrestoBlue™, Thermofisher Scientific) was used to evaluate the activity of pmTECs and HUVECs in different culturing conditions (Table 1). Cells were seeded in 2D at a cell density of 10000 cells/cm^2 in a non-treated multiwell previously coated, as previously described for the expansion of pmTEC. The

Table 1
Different combination of cells and culture medium used for co-culture condition screening with metabolic activity assay.

Cell type	Culture medium	Nomenclature
pmTEC	DMEM/F-12 supplied with growth factors	pmTEC in DMEM-GF
HUVEC	endothelial cell growth medium	HUVEC in EGM-2
pmTEC	endothelial cell growth medium	pmTEC in EGM-2
HUVEC	DMEM/F-12 supplied with GF	HUVEC in DMEM-GF
50:50 pmTEC-HUVEC	DMEM/F-12 supplied with GF	50:50 pmTEC-HUVEC in DMEM-GF
50:50 pmTEC-HUVEC	endothelial cell medium	50:50 pmTEC-HUVEC in EGM-2
pmTEC	50:50 DMEM/F-12 supplied with GF:endothelial cell medium	pmTEC in 50:50 DMEM-GF:EGM-2
HUVEC	50:50 DMEM/F-12 supplied with GF:endothelial cell medium	HUVEC in 50:50 DMEM-GF:EGM-2

resazurin-based solution was incubated and metabolized by viable cells and converted into a red fluorescent solution that can be detected using fluorescence or absorbance measurements. Triplicates for each condition were measured on day 1, 3, 7 and 14. Incubation period of 30 min and 2 h were evaluated. Resazurin-based solution was used as control and the measured fluorescence levels were subtracted to the tested cellular conditions.

Furthermore, a second metabolic study was performed on 3D droplets ($n = 3$) of C_alginate, IH_alginate and pectin containing HUVECs cultured in EGM-2 for 1, 3 and 7 days, at a cell density of 2×10^6 cell/ml. At each timepoint samples were incubated for 2 h with resazurin-medium solution and the fluorescence of the supernatant measured. Hydrogel droplets incubated with resazurin-based solution were used as control and the measured fluorescence level were subtracted to the tested droplets with encapsulated cells.

The measurements were made using a plate reader (CLARIOstar-BMG, Labtech), using an excitation wavelength of 550 nm and an emission wavelength of 590 nm.

2.10. Core-shell microfluidic bioprinting

A novel core-shell printhead, a prototype version of the CENTRA printhead (Aspect Biosystems, Canada) was used to bioprint core-shell filaments (Fig. 2a). A 2% w/v gelatin solution prepared in PBS was mixed with pmTEC (25×10^6 cells/ml) and bioprinted as filament core and a commercial alginate/fibronectin (200:1) with HUVECs (4×10^6 cells/ml) was bioprinted as filament shell. A post-crosslinking process for 5 min was performed, by immersing the constructs in a sterile filtered 125 mM $CaCl_2$ solution prepared in milliQ water. HUVECs were stained in blue using a cell tracker (ThermoFisher Scientific, blue CMAC dyes) to facilitate the imaging analysis or the bioprinted core-shell filaments. The bioprinted filaments were then imaged on different days, i.e. day 0 (right after bioprinting), 1, 2, 7, 14, 21 and 28, using the SlideScanner microscope (Nikon eclipse Ti, Japan). On each timepoint, a new sample was investigated.

Finally, the core-shell constructs were fixed with 4% PFA and imaged using the confocal microscope (Leica TCS SP8 STED) to observe the reorganization of cells inside the hollow filament over the culture period.

2.11. Statistical analysis

The statistical analysis was performed using the software GraphPad Prism8 (version 8.2.0). A statistical significance study was conducted performing a one-way ANOVA test, with a Tukey's multiple comparisons test. A P value smaller than 0.05 ($P < 0.05$) was considered statistically significant (*).

3. Results and discussion

3.1. Primary cell isolation and characterization

Most studies use cell lines or immortalized cells for 3D *in vitro* systems as they are generally highly proliferative and easier to culture [24]. In contrast to cell lines, primary cells which are directly isolated from tissue, have a finite lifespan and limited expansion capacity. But primary cells have in contrast to cell lines a normal cell morphology and maintain many of important markers and functions [25]. Primary cells isolated from tissue exhibit not only normal physiology, whereas cells immortalized with adenoviruses expressing EBV, SV40 T antigens, p53 or hTERT showed no signs of senescence, but also give the possibility to analyse further factors such as age, medical history, and sex. With a growing trend towards personalized medicine, such donor variability and tissue complexity can only be achieved with use of primary cells and are difficult to replicate with cell lines that are very systematic and uniform in nature and do not capture the true heterogeneity of a living tissue. Because primary cells are more relevant and reflect the *in vivo* situation better, we decided to isolate primary cells for our 3D *in vitro* model. Although primary human cells would be the best to build an artificial kidney-like 3D *in vitro* model to explore pathomechanisms of human renal diseases, the isolation possibilities are limited. One of the most important reasons is the low availability of tissue. Furthermore, the only possibility to get tissue (e.g. from healthy patients) is during tumour enucleation or from organs not suitable for transplantation. Both of these cases occur rarely, which limits the procurement of healthy tissues. In addition, tubular cells are highly vulnerable to hypoxia therefore time until the isolation has to be short. Murine animal models are frequently used in research to analyse renal diseases. Therefore, we have started with murine primary cells with the advantage of the availability of cell-specific reporter mice.

The focus of this study was to bioprint renal tubular epithelial cells as these are the major cell type present in the kidney, sensitive to several injuries and with a high regenerative capacity. Keratins (K) are intermediate filaments specifically expressed in epithelial cells, including the renal tubular cells, and are therefore widely used as specific epithelial biomarkers. Taking advantage of this, a transgenic K8-YFP mice was used to isolate several primary murine cells with focus on tubular cells (pmTECs) [26]. This presence of K8-YFP allowed to prove the origin of the cells and facilitated the visualization of the cells inside a complex structure without fixation or staining of the cells. Further, K8 reporter cells enabled a monitoring over the culturing period.

To prove the functionality of the transgenic mice, transgenic and wildtype animals underwent unilateral ureteral obstruction (UUO) as a model of renal fibrosis. K8-YFP expression was analysed in cryosections and compared to immunohistochemistry for K8 expression in wildtype mice. The expression pattern of K8-YFP was specifically confined to tubular epithelial cells in both healthy and fibrotic kidneys. The K8 expression pattern of the reporter mice was the same as in wildtype mice. We have shown previously that keratins are early markers of tubular injury and become significantly upregulated in UUO [27]. Confirmatory, K8-YFP expression was also increased in fibrotic UUO kidneys similar the K8 expression in wildtype mice (Fig. 1a). For isolation of several different cell types at once a combination of different isolation protocols was tested. After tissue lysis and sieving, selection of different cell types was performed by selective media or by FACS sorting (Figure S1a). FACS sorting for endothelial cells was performed with antibodies against CD31 as an endothelial specific marker. Some cells could be sorted by this method, but were not viable (data not shown).

FACS sorting of the freshly isolated YFP-cells was tested (Figure S1b). Interestingly, only 5.8% of kidney cells were YFP-positive and the signal intensity was weak. Analysis of the K8-YFP cells directly after the isolation procedure and during 15 days revealed a strong loss of signal directly

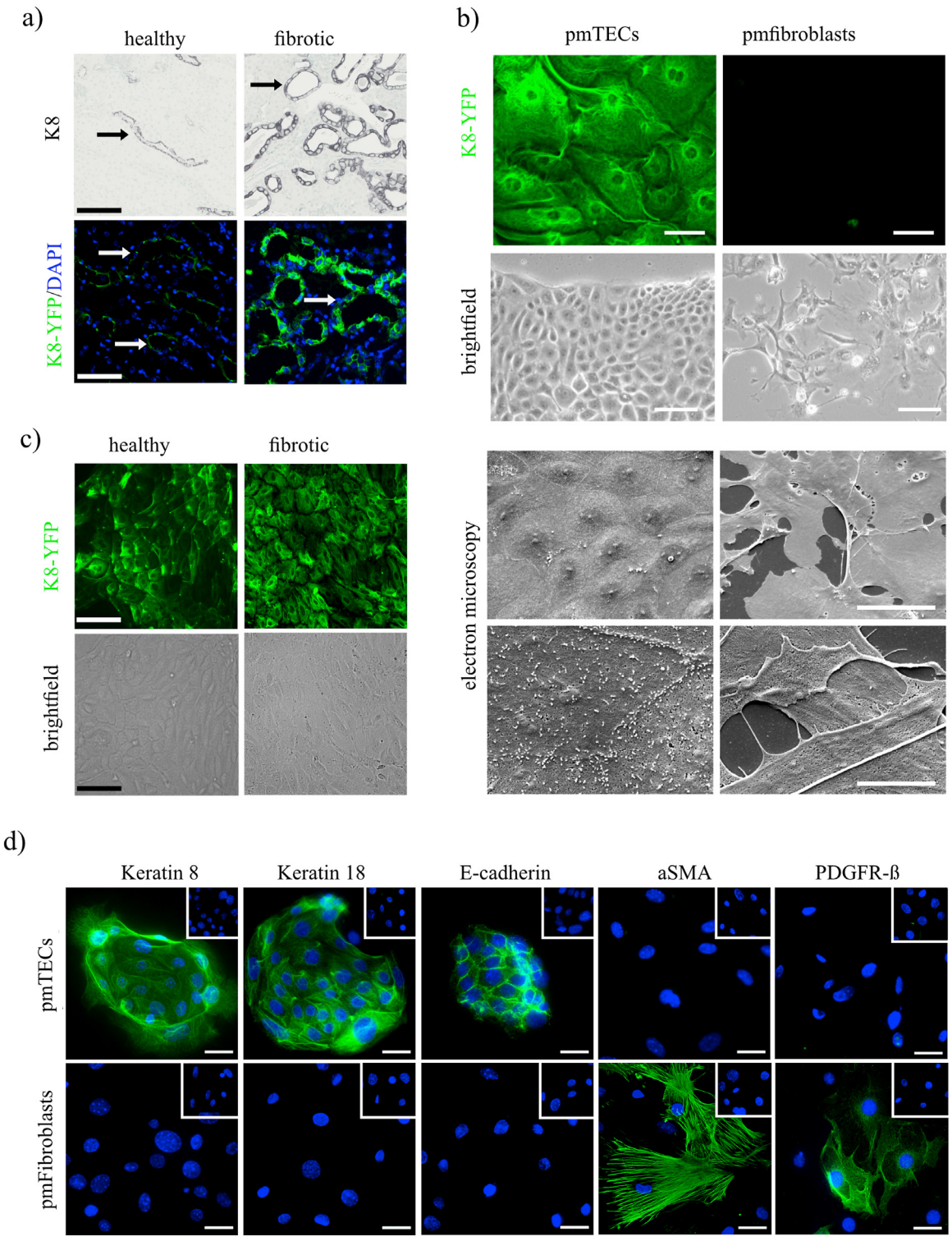

Fig. 1. Characterization of primary renal tissue of healthy and fibrotic kidneys: a) wildtype and K8-YFP mice underwent unilateral ureter obstruction (UUO) for 5 days. Immunohistochemisty of keratin (K) 8 in wildtype mice showed increased expression in fibrotic kidney compared to healthy contralateral kidney. Similar increase was found in K8-YFP mice analysing the K8-YFP fluorescence signal (Green). Scale bar = 100 µm. b) Primary murine Fibroblasts (pmFibroblasts) and primary murine tubular epithelial cells (pmTECs) have been isolated by selective media from K8-YFP mice. Isolated K8-YFP pmTECs showed stable epithelial phenotype and typical keratin distribution pattern with strong fluorescent signal, whereas isolated primary (pmFibroblasts) showed no K8-YFP expression and a spindle shaped appearance. Scale bar = 100 µm. Epithelial characteristics such as cobble stone growth and microvilli were also visible in electron microscopy (scale bar = 5 and 50 µm). c) Isolated pmTECs from healthy kidneys showed fine fibers of the keratin network, clear cell borders and cobblestone formation, whereas primary murine TECs isolated from fibrotic UUO day 5 demonstrate already a morphological change to a more spindle shaped appearance of the cells and a keratin network with bundled fibers. Scale bar = 100 µm. d) Compared to pmFibroblasts isolated with the same method, pmTECs were positive for all tested epithelial markers, including Keratin 8 (K8), Keratin 18 (K18) and E-cadherin and were negative for α-SMA and PDGFR-β representing markers for fibroblasts, whereas pmfibroblasts were only positive for α-SMA and PDGFR-β. Negative control for each staining is depicted in the inlay in the right corner. Scale bar = 25 µm.

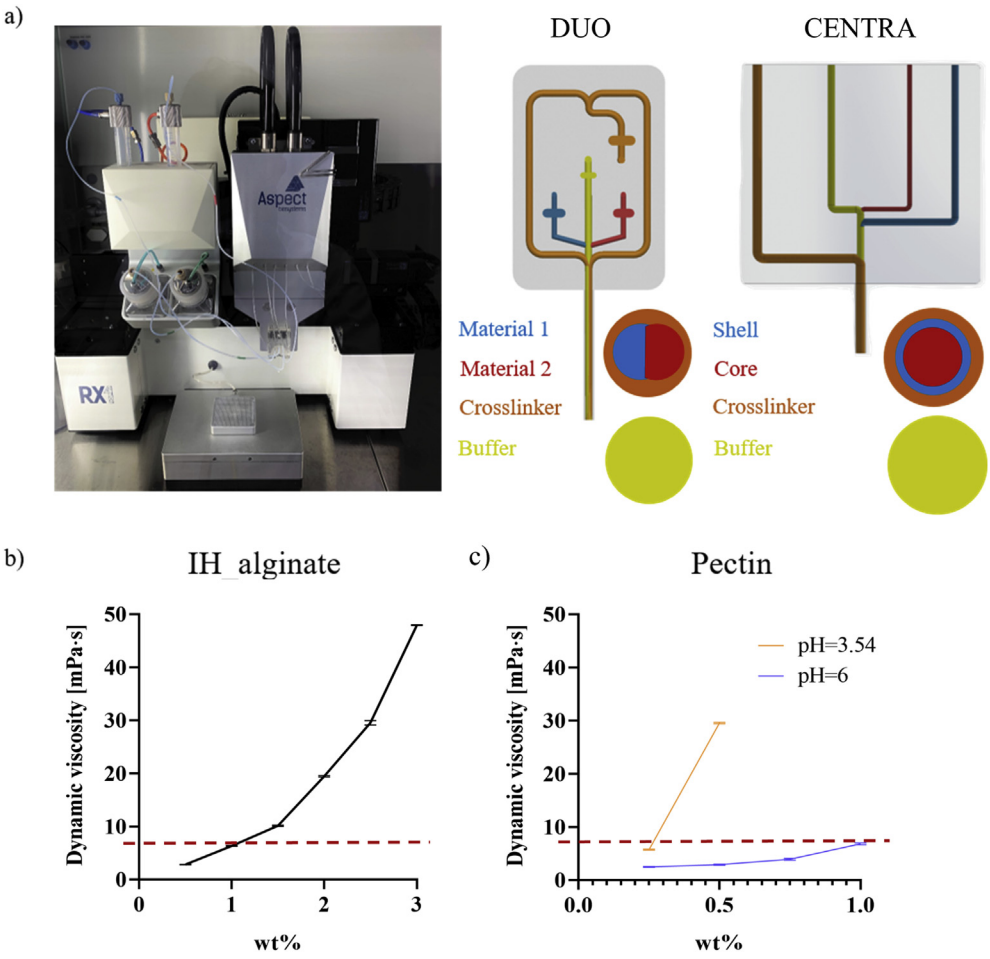

Fig. 2. Microfluidics 3D bioprinter and printheads used, and viscosity characterization of investigated biomaterial ink solutions. a) RX1Bioprinter (Aspect Biosystems). Schematic of the two printheads used, i.e. DUO and a prototype version of CENTRA core-shell printhead and cross section of the nozzle during bioprinting. Each bioprinting session is conducted by co-extruding material 1/shell, material 2/core with the crosslinker for the DUO/prototype CENTRA printheads respectively. At the end of the bioprinting session, the buffer solution is extruded. b) Viscosity of the in-house alginate (IH_alginate) solution as function of concentration, c) viscosity of pectin solution as function of concentration and pH. The red dash line indicates the average viscosity of the commercial alginate (C_alginate) solution.

after isolation, which starts to gradually recover after the first 24 h (Figure S1c). This suggested potential inactivation of the fluorescent reporter protein, perhaps due to the rearrangement of the intermediate filaments during the isolation process. Therefore, FACS-based isolation seemed not to be useful isolation technique, also due to additional cell stress during the FACS. To check if loss of YFP signal can also be observed during normal cell passaging, K8-YFP cells were monitored during the trypsinization (Figure S1d). In contrast to the isolation procedure, adding trypsin did not alter the signal. In some detached cells, the K8-YFP signal was even stronger most probably due to a condensed intermediate filament network.

An alternative isolation method for pmTEC, endothelial cells and fibroblasts from healthy K8-YFP mice using selective media promoting growth of the specific cell types was tested. A culture media supplemented with EGF and without FCS to select for epithelial cells was used. In parallel, cells were cultured in DMEM supplemented with 10% FCS to promote fibroblast growth and in EGM2 medium to promote endothelial cell growth. Cells cultured for three passages in the EGF supplemented media showed the typical cobblestone shaped of epithelial cells growing in a confluent monolayer, whereas fibroblasts cultured in the FCS supplemented media showed typical spindle-shaped morphology and non-confluent growth (Fig. 1b). Endothelial cells cultured in EGM2 medium were divergent in shape and appearance and stopped proliferating already before the first passaging (data not shown).

Analysis of the fluorescence signal of K8-YFP after three passages revealed more than 99% of the cells in the rEGF supplemented media were positive, confirming the specificity of this isolation technique for pmTECs. In the FCS supplemented media, less than 2% were YFP-positive, confirming the predominance of non-epithelial cells. Electron microscopy showed typical features of epithelial cells such as microvilli. Both cell types could be grown over several passages (>9).

Additionally, it was tested if isolation of primary cells was possible also from diseased fibrotic kidneys. For future work primary cells isolated from a fibrotic environment will be a relevant cell source to further understand molecular pathways leading to disease progression. Due to the K8-YFP reporter mice focus was on the TECs. Cells from a healthy kidney showed the expected cobblestone shape in brightfield and a fine, regular filament network in fluorescent microscopy (Fig. 1c). Tubular cells isolated from the fibrotic kidney showed less cobblestone and more spindle-shaped appearance, in line with the morphological appearance of injured tubules in the UUO model, with a more irregular filament network. These morphological changes could already hint to an activated or injured state of the pmTECs, which would be expected after UUO.

Confirmation of the specific isolation of pmTECs and fibroblasts using the selective media was performed by staining for epithelial markers such as Keratin 8, Keratin 18 and E-Cadherin, and classical fibroblast marker alpha-smooth muscle actin (αSMA) and platelet-derived growth factor receptor beta (PDGFR-β) (Fig. 1d). Taken together, we established a relatively fast and easy method to isolate pmTECs and fibroblasts in parallel and further optimization is necessary for the culture of endothelial cells. K8-YFP pmTECs seem to be a useful tool to prove the epithelial origin and to visualize the cells during the experiment, which might be particularly suitable for *in vitro* models to monitor the cells over the culture period. Changes in the K8 filament network can also hint to cellular stress as a potential direct read-out in such models. Therefore, we used K8-YFP pmTECs to establish our bioprinting method. These cells can be monitored continuously to evaluate cell organization inside bioprinted constructs without the need for further staining. For future work, transgenic mice with several reporter genes each specific for the cell type of interest are envisaged.

3.2. *Characterization of the biomaterial ink*

The microfluidic 3D bioprinter (Fig. 2a) uses air pressure as a driving

force for the extrusion of the solutions. Therefore, viscosity is one of the most important parameters to be tested to ensure printability. The viscosity of IH_alginate and pectin was compared to the viscosity of C_alginate. The latter viscosity was used as reference (dashed line in Fig. 2b and c) for the production of IH_alginate and pectin, ensuring the extrusion of solutions, avoiding the clotting of the printhead. The viscosity of the IH_alginate was tested in a concentration range of 0.5 – 3 wt %. For the pectin solutions, a concentration range of 0.25–1 wt% and two pH conditions (pH 6 and pH 3.54) were tested (Fig. 2c). Concentrations above 0.5 wt% prepared with a pH of 3.54 showed a high viscosity outside of the measurable range. For the alginate, the pH was not investigated as the viscosity is not greatly affected as reported in literature [28]. The investigated ranges were selected to determine the ideal concentrations to mimic the viscosity of C_alginate. A 1 wt% IH_alginate solution exhibited a similar viscosity as the reference C_alginate solution (Fig. 2b). However, the stability of the filaments produced with 1 wt% IH_alginate was low. Therefore, a 2 wt% formulation was further used, even if the viscosity was 2-fold higher in comparison to the commercial solution. The difference in crosslinking between these two IH_alginate concentrations used may be explained by the higher dispersion of molecules in solution, which require a longer exposure to the crosslinker to obtain a stable filament. The relatively short period of contact between the biomaterial ink and the crosslinker solutions in the printhead might explain the insufficient stability of the filaments manufactured with 1 wt % IH_alginate solution.

Whereas the dynamic viscosity of the IH_alginate solution demonstrated an exponential-like behaviour in relation to the concentration (Fig. 2b), confirming results found in literature, the pectin solution showed a more linear-like increase (Fig. 2c). This result is in line with the literature showing that the viscosity of pectin increases as the concentration increases [20,23,29]. The influence of pH on the viscosity of pectin solution in our experiment was also comparable to published results showing that an increase in pH resulted in a decrease of viscosity [21]. It is well documented that the polymeric chain breaks down at higher pH leading to degradation of the pectin, and thereby to decreased viscosity and stability [19,22]. With increasing pH the charge density of pectin molecules increases as well, resulting in higher electrostatic repulsion among pectin molecules which limits the gel formation [30]. A pH of 6 was shown to provide a good hydrogel formation with a good scaffold stability and high cell viability up to 21 days [18]. For all further experiments a pectin solution of 1 wt% with pH = 6 was used.

Alginate biomaterial inks molecular weight (MW) and polydispersity index (PDI) was measured. PDI is the measure of the molecular weight distribution and it is calculated with the ratio between weight average molar mass and number average molar mass. The MW and PDI of C_alginate was equal to ~186 kDa and 2.12, whereas the IH_alginate was ~210 kDa and 2.65, respectively. Both biomaterial inks show a similar MW and PDI correlating with the close bioprinting resolution observed for both as reported below. In literature, similar bioprinted approaches have used alginate with a MW of ~33 kDa [31,32]. This lower MW alginate was blended with PEG and fibrinogen [31], or GELMA and methacrylate hyaluronic acid [32] to ensure suitable rheological properties for bioprinting. Having a higher MW alginate generally increases the viscosity of the biomaterial ink solution, thus affecting the microfluidic bioprintability of the biomaterial ink. In this study, an alginate-only solution, i.e. not blends, was selected to have a better control on the bioprinting process.

3.3. Optimization of the processing parameters and manufacturing of 3D structures

A multitude of bioprinting techniques is nowadays available. Microfluidic bioprinting has several advantages, i.e. high monodispersity, high reproducibility, the possibility to bioprint different shaped-constructs composed of filaments ranging from 0.1 to 1 mm in diameter and the versatility in the co-extrusion of different biomaterial inks or bioink formulations [1,33]. Furthermore, with the microfluidic bioprinting systems used in this study, a shield fluid is used to reduce the shear stress applied to the cells, as these are not in direct contact with the inner surface of the printhead nozzle.

To evaluate the influence of the diverse processing parameters on the obtained filament diameter, quality of the filaments and overall structures, a parametric study was performed for the three tested biomaterial inks (Fig. 3). The following processing parameters were analysed: i) crosslinker pressure ii) material pressure, iii) translation velocity and iv) offset. With an increase of the crosslinker pressure or the translation velocity, a decrease in the diameter of the extruded filament was observed for all three analysed biomaterial inks. Conversely, an increase in the material pressure induced an increase in the filament diameter, also independently of the biomaterial ink. An increased offset resulted in the production of filaments with a smaller diameter for the pectin and the C_alginate solution, whereas no clear trend was observed for the IH_alginate (Fig. 3b). The offset in the current system is manually set, increasing the possibility of user-dependent errors. Hence, the possible limitation of observing a clear trend on the influence of the offset parameter.

The obtained results for the four processing parameters were expected due to the nature of the bioprinting process. The DUO printhead has fixed channel dimensions, nozzle diameter and the dimension of the bioprinted filaments is depending on the processing parameters evaluated. The pressure and volume flow are dependent of the solution viscosity. A laminar fluid flow is maintained inside the printhead nozzle ensuring a uniform filament diameter while ensuring a relatively accurate deposition. Furthermore, the stability of the filaments produced with C_alginate with an offset below 190 μm was limited, thus the handling of such filament for analysis was impossible (Fig. 3a). For the pectin solution, a material pressure below 20 mbar allowed the manufacturing of filaments of smaller diameter, although these were not stable enough to be analysed (Fig. 3c).

Previous studies tested in-house multichannel coaxial extrusion system [31,32,34–38]. This system is equipped with a microfluidic printhead, allowing a rapid deposition and switching among multiple biomaterial inks or bioinks. The main difference among the microfluidic printheads used in literature is how the crosslinker is extruded, either perpendicular or concentrically to the nozzle. Syringe pumps that are connected to the inlet of the printhead in the coaxial extrusion nozzle control the extrusion flow rate. The microfluidic bioprinter used in this study has a built-in pressure controlled system, which induces the flow of the biomaterial inks or bioink from the reservoirs to the printhead. In the literature, the same commercial microfluidic bioprinter was used and the obtained filaments had a dimension of approximately 300 μm [39]. These diameters were obtained by bioprinting C_alginate doped with either collagen I or intestinal decellularized extracellular matrix (dECM), together with a commercial crosslinker and applying a pressure of 45 mbar to each channel [39]. Similarly, a mixture of alginate-GelMA (viscosity of 80 mPa/s) was bioprinted using a different microfluidic bioprinter, where the mixture is crosslinked with a 300 mM $CaCl_2$ solution. This resulted in filaments with a diameter in the range of 150–300 μm depending on the deposition speed, 1 mm/s and 6 mm/s respectively [36]. Finally, a coaxial extrusion system was reported to fabricate alginate fibers with 200 μm diameter [40]. The interplay between processing parameters and the results obtained herein are therefore in line with the literature.

An average filament diameter of approximately 200 μm was aimed to ensure suitable nutrient/oxygen diffusion across the filament without a present vascularization to ensure cellular viability and metabolic activity [35,41]. The bioprinting parameters obtained from this parametric study to produce filaments with 200 μm for the different biomaterial inks are reported in Table 2. These optimized parameters were used to bioprint 3D structures, such as cylinders and cubes, proving the capability to bioprint different macro sized-constructs. These layer-by-layer structures are obtained extruding continuously the filament with the optimized

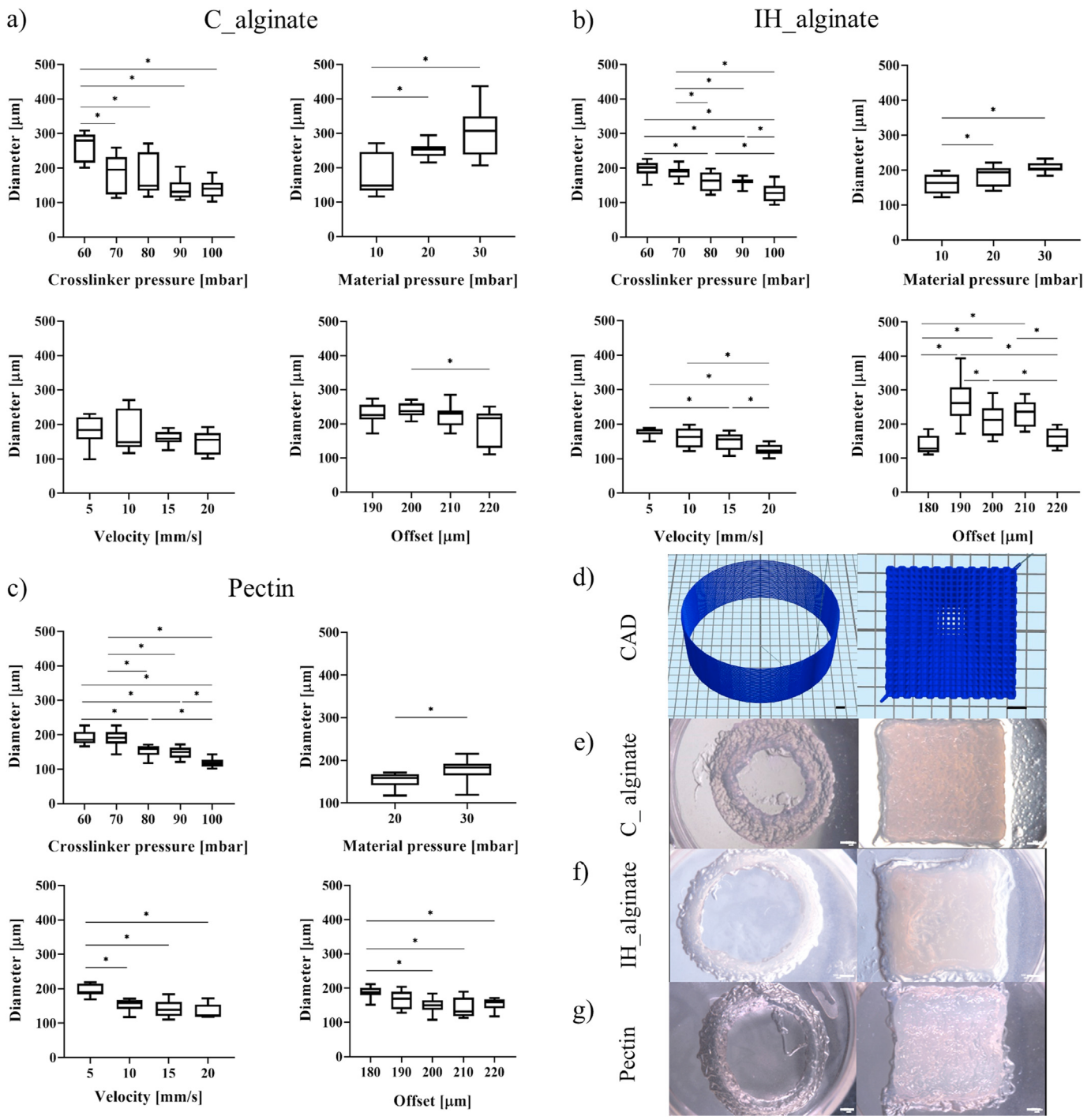

Fig. 3. Evaluation of the influence of the bioprinting parameters on the diameter of the extruded filaments for: a) commercial alginate (C_alginate), b) in-house alginate (IH_alginate) and c) pectin. d) CAD 3D representation of the hierarchical structures manufactured with optimized conditions made of e) C_alginate, f) IH_alginate and g) pectin. Statistically significant differences (*) for $p < 0.05$ are highlighted. Scale bar = 1 mm.

processing parameters. These structures showed the capability to manufacture large-size 3D structures, in the mm range (Fig. 3d, e, f, g). As the construct builds up in size and thickness, an instability over the filament deposition is observed reducing the accuracy of the obtained constructs. The structures manufactured with C_alginate, IH_alginate, and pectin showed filaments deposited with some visible defects and with a limited identification of the woodpile structure initially designed. These artefacts could be induced with an accumulated error of the interlayer offset or the accumulation of the crosslinking solution while the constructs build up in thickness. Furthermore, the limited degree of shape fidelity might be due to low chosen viscosities of the biomaterial inks (Fig. 2), since it is known that higher-viscosity materials (>30 mPa*s) provide better structural support for the manufactured structures [42]. However, these high viscosities show limited processability in the microfluidic bioprinter with the printhead used in this study. It has been

Table 2
Optimal bioprinting parameters obtained for the bioprinting of commercial alginate (C_alginate), in-house alginate (IH_alginate) and pectin biomaterial inks.

Biomaterial inks	Crosslinker pressure [mbar]	Material pressure [mbar]	Velocity [mm/s]	Offset [µm]
C_alginate	80	10	10	220
IH_alginate	80	10	10	220
Pectin	80	20	20	210

reported that for these high viscosity values some degree of clotting of the biomaterial inks inside the printhead can occur [39,43].

3.4. Cell viability on bioprinted constructs

Analysis of cell viability was performed on bioprinted 3D structures and on droplets, containing either primary isolated tubular cells from K8-YFP mice or HUVEC cells. Both cell types were tested in combination with the three different biomaterial inks, C_alginate, IH_alginate and pectin (Fig. 4). The bioprinted structures were bioprinted using the DUO printhead. The manually pipetted droplets served as controls to evaluate cell viability of unprocessed bioinks.

The live/dead assay demonstrated a high viability in bioprinted constructs (Fig. 4b, d) as well as in droplets (Fig. 4a, c). No noticeable difference in viability was observed between HUVEC and pmTEC cells as shown in Fig. 4a and b vs. Fig. 4c and d respectively. Both cell types had viability above 91% for the alginate solutions and above 82% for the pectin solution on day 7. In literature, viability of 91.65 ± 6.85% on day 6 was reported for bioprinted constructs with hiPSC-derived neural aggregates in fibrin-based scaffolds, using the same microfluidic bioprinter platform [43]. This demonstrates that primary isolated cells, at least pmTECs, are useable for bioprinting and show similar viability as cell lines. To the best of our knowledge, this is the first time bioprinting of primary tubular epithelial cells is reported. In previous reported studies, immortalized proximal tubular epithelial cells were bioprinted [14,16], or human primary glomerular microvascular endothelial cells have been used [11].

The overall structural stability of the bioprinted constructs gradually decreased during culture due to the gradual depletion of Ca^{2+} ions (Figure S2). Taking into consideration the low concentration of alginate and pectin solutions used to produce the bioink, a gradual migration of cells to the surface was observed during culture (Fig. 4). After seven days in culture, the constructs were still stable, but the change of culture medium gradually reduced the crosslinking of the constructs, and some signs of low stability areas were observed.

IH_alginate was produced in PBS, as ideal environment in terms of osmotic balance and pH stability for the cells while bioprinting. The stability of the bioink can be overcome by increasing the crosslinking concentration, the crosslinking time and eventually performing different crosslinking periods along with the culture. Other strategies such as increasing the polymer concentration might as well reduce the degradation rate and increase the stability of the constructs during long-term cultures. Accordingly, an increase of concentration can rise the viscosity of the bioink, and this can be a limit in microfluidic 3D bioprinter as previously described. Furthermore, the use of alginate solution in PBS is contradictory in literature. It is known the phosphates present in PBS bind to the calcium ions reducing alginate mechanical integrity [44], while other studies report no issue in terms of stability of alginate scaffolds in PBS [45].

For the pectin, the concentration of 1 wt% used was smaller when compared with previously reported studies where 2.5 wt% was used to produce disc hydrogels [18]. Furthermore, in the same report a $CaCO_3$/GDL crosslinker solution where the GDL hydrolyses with time, triggering the slow release of Ca^{2+} from $CaCO_3$ molecules, whereas the $CaCl_2$ commercial crosslinker lacks this sustained release of calcium ions [18]. Other examples report a post-crosslinking after bioprinting during a period of 5 min allows the increase of the construct stability over the culture period, without affecting the viability of the bioprinted cells [46].

As the formation of pectin hydrogels can be largely affected by pH variations, evaluating the results obtained with the live/dead assay, it was clear that the buffer solutions can negatively affect the stability and integrity of the bioprinted constructs. As upon completion of the bioprinting process, a washing step of the printhead inner channel is automatically done in the deposition area of the construct. This step might have reduced the overall exposure of the bioprinted construct to the crosslinker. However, we were able to maintain stability over seven days of culture. Additional post-crosslinking strategies could further increase the stability of the bioprinted constructs if longer culturing periods are aimed.

3.5. HUVECs and pmTECs co-culture conditions

To manufacture core-shell constructs with HUVECs and pmTECs in parallel, an initial screening to identify suitable culture conditions for the co-culture was performed. Metabolic activity and cell morphology evaluation were performed during 14 days of culture (Fig. 5, Figure S3, Figure S4). The cell morphology was monitored by brightfield (HUVECs, pmTEC) and fluorescence imaging (pmTEC) at the day 1, 3, 7 and 14 (Figure S3).

The standard culture medium for pmTECs (DMEM-GF, DMEM supplemented with the growth factor EGF) and the endothelial cell growth medium (EGM-2) as well as a 50:50 mixture of both media were tested for both cell types alone or in a 50:50 co-culture. A limited growth and a gradual death of HUVECs when cultured in tubular-specific DMEM-GF was observed. This was also confirmed by the absence of a measurable metabolic activity (Fig. 5, Figure S3f and Figure S4). This can be explained due to the lack of vascular endothelial growth factor (VEGF) in the DMEM-GF, which is essential for HUVECs proliferation. Conversely, pmTECs were able to proliferate in the endothelial specific EGM-2 medium and maintain the keratin expression for the 14 days in culture, although with lower metabolic activity when compared with DMEM-GF medium (Fig. 5, Figure S4). EGM-2 medium contains EGF, explaining the capability of the pmTEC to proliferate in this medium. This could also explain why separation of primary endothelial cells with EGM-2 medium was not sufficient and several different cell morphologies were detectable. HUVECs culture in a 50:50 mixture of the two different culture media showed no statistically significant difference when compared with only EGM-2 medium on day 14. The pmTEC metabolic activity in the 50:50 medium mixture was within the same range of endothelial-specific DMEM-GF alone. For co-culture conditions of both cell types in a 50:50 ratio, the metabolic activity in DMEM-GF was significantly lower than in EGM-2 medium (Fig. 5, Figure S4). Taken together, we concluded that HUVECs require their specific medium to grow, with VEGF as a fundamental growth factor, confirming the results of published studies [47]. These results allowed us to identify the best culture conditions to culture the bioprinted core-shell filaments following described. Further analyses should be performed to evaluate if cell phenotypes are preserved in these culture conditions.

The metabolic activity of encapsulated cells was initially evaluated on droplets containing HUVECs with the resazurin-based assay (Figure S5). This condition was selected as the values measured with HUVECs culture with EGM-2 showed the highest metabolic activity. The values of fluorescence were drastically reduced on encapsulated cells due to the reduced diffusion of the resazurin-medium solution and the resorufin through the hydrogels. Furthermore, the fluorescence per number of cells was measured for the HUVECs cultured in EGM-2, on day 1, after 2 h incubation period. The difference of detected signal between the cells cultured in the droplets and monolayers was investigated for all three bioinks (Figure S6). The IH_alginate was shown to be the bioink with the lowest diffusion of resazurin and metabolized resorufin (Figure S6a), in which the encapsulated cells metabolized and excreted the resorufin showing a fluorescent signal 700 times smaller than the fluorescence values measured for the HUVECs monolayer (Figure S6b). Further studies to analyse other conditions of cells cultured in droplets and monolayers were not investigated due to the reduced fluorescent intensity observed in the tested condition of HUVECs cultured in EGM-2.

3.6. Core-shell bioprinting

The novel prototype version of the CENTRA printhead allowed to accurately manufacture core-shell filaments with the possibility to control the deposition of the bioprinted cells, the overall filament size and

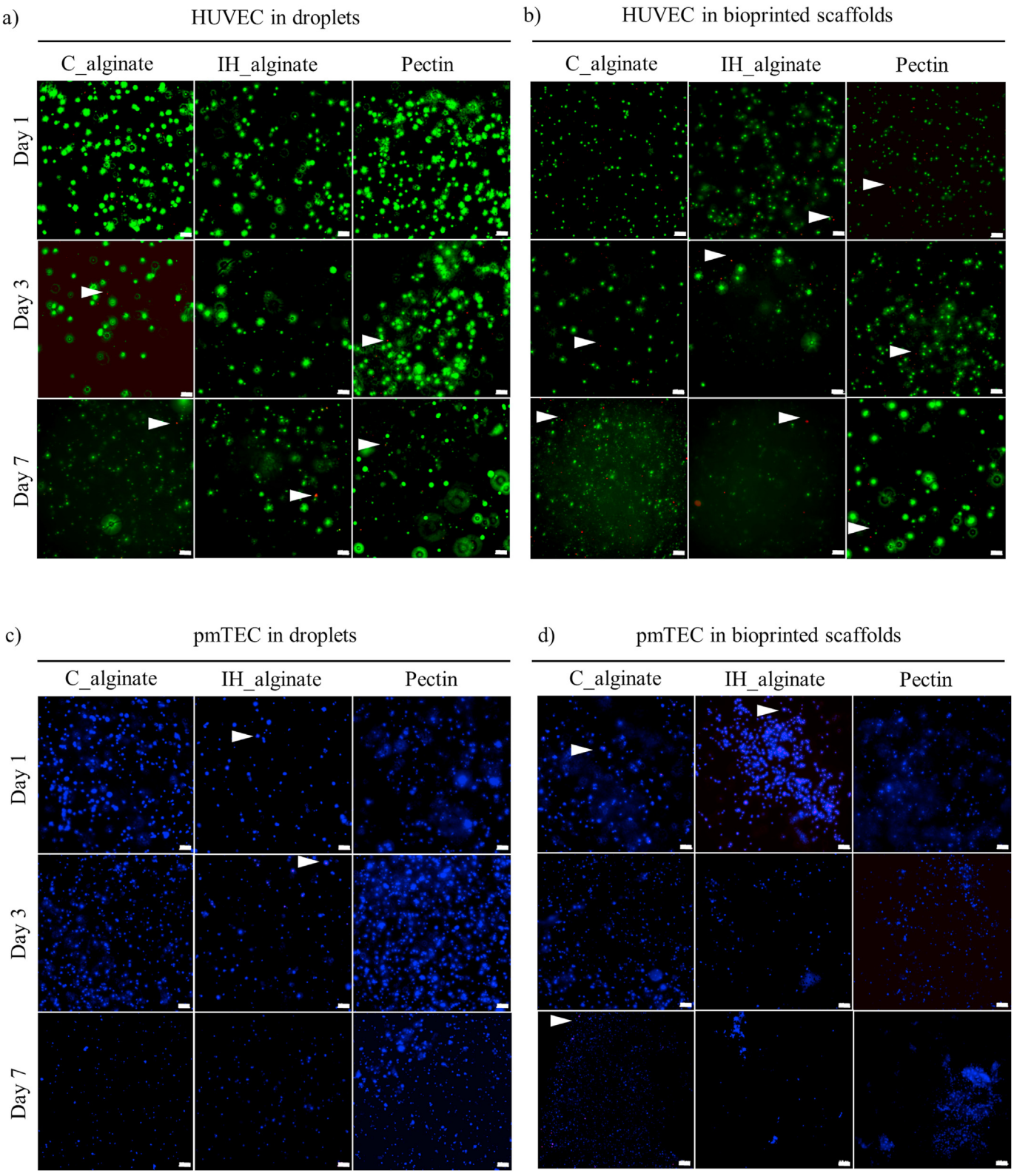

Fig. 4. Cell viability assay performed on droplets and bioprinted constructs (viable HUVECs were stained with calcein green AM and pmTEC stained with calcein blue AM and with EthD-1 for dead cell for all the conditions) manufactured with commercial alginate (C_alginate), in-house alginate (IH_alginate) and pectin: a) HUVEC in droplets, b) HUVEC in bioprinted scaffolds, c) pmTEC in droplets, d) pmTEC in bioprinted scaffolds. The white arrows highlight dead cells. Images represent a deconvoluted z-stack maximum intensity projection. Scale bar = 100 μm.

the core-shell dimensions by varying the process parameters such as the pressure for each channel. To allow continuous monitoring of the bioprinted filaments during culture, HUVECs (stained in blue) were homogeneously distributed in the commercial alginate-fibronectin bioink in the outer shell, while the pmTECs (stained in green) were mixed with gelatin to form the core bioink. The C_alginate was used as it demonstrated improved stability of the constructs over the culture period, as highlighted before (Fig. 4). The combination of C_alginate and fibronectin was chosen considering the composition used to culture pmTECs in 2D and to circumvent the lack of adhesion sites in the alginate. Gelatin was chosen to exploit its sol-gel transition at 37 °C, giving the stability to form a core-shell filament during the bioprinting process

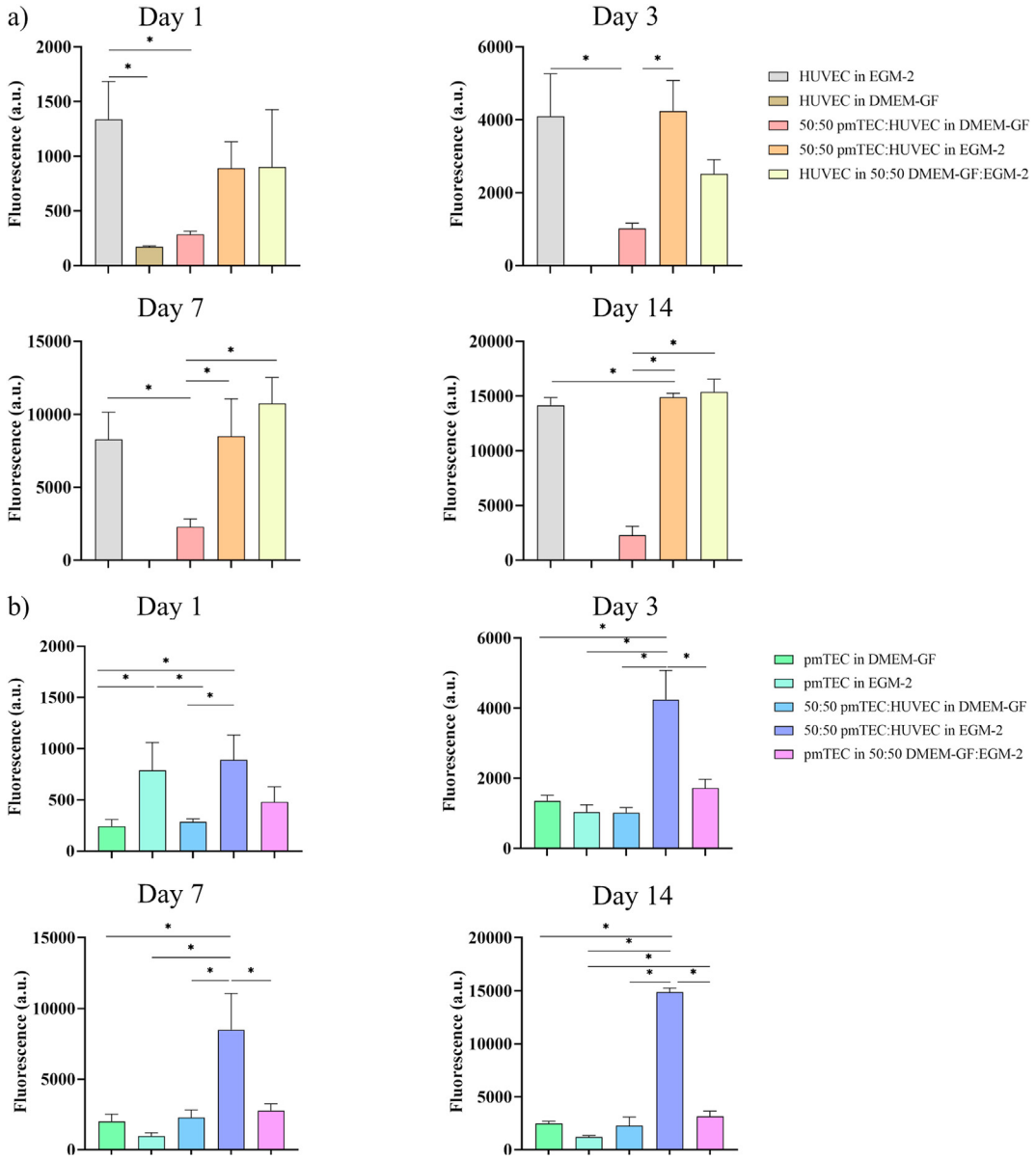

Fig. 5. Metabolic activity measurements testing different combinations in terms of cell types and cell media (Table 1), with a fixed incubation period of 2 h. Measurements were made on day 1, day 3, day 7 and day 14. a) Analysis of the metabolic activity for the culture of HUVEC; b) analysis of the metabolic activity for the culture of pmTEC. Only positive values of fluorescence are plotted. Statistically significant differences (*) for $p < 0.05$ are highlighted.

at room temperature (21.5 °C) and then being gradually washed away once placed in the incubator at 37 °C, possibly forming a hollow filament. This would allow mimicking the renal tubule.

The first step for the production of the core-shell filaments was the optimization of the bioprinting parameters taking the values previously optimized for the DUO printhead and changes in the channel diameter into account (Fig. 3). Combinations of crosslinker pressure (200 mbar), core pressure (150 mbar), and shell pressure (100 mbar) were used. The capability to bioprint precisely the green-stained pmTECs in the core and the blue-stained HUVECs in the shell is shown in Fig. 6a. The bioprinted samples were cultured using only EGM-2, following the result obtained for the metabolic activity study. The core-shell filaments were then imaged using a confocal microscope, showing the formation of a hollow filament over the culture period (Fig. 6b). In particular, the sample from day 14 showed the distribution of cells in the core of the filament after the remodelling of the gelatin supportive bioink used in the core.

The average external diameter of the core-shell filaments was 450.84 ± 9.17 μm, bigger than the filaments obtained with the DUO printhead, considering the core-shell printhead has a nozzle with a bigger diameter. The core-shell filaments obtained herein are smaller than the filaments reported in the literature, where diameters up to 2 mm were achieved, showing an increased in resolution and accuracy in dimension of the bioprinted filaments [16,48–50]. To our best knowledge, these are the smallest core-shell filaments produced with a microfluidics bioprinter reported in the literature, but further optimization is necessary to obtain filaments within the range of the tubule diameter in the human kidney [51].

The core-shell printhead was used to demonstrate the possibility of manufacturing a concentric arrangement of the two different cell populations envisioning an *in vitro* model able to mimic the proximal renal tubule and the intricate exchange with the vasculature in the vicinity of the tubules. In particular, the core-shell is the most appropriate arrangement to produce a proximal tubule wrapped by endothelial cells that upon appropriate stimuli can form a capillary network, maximising the diffusion of oxygen and nutrients towards the epithelial cells, mimicking the *in vivo* environment. The combination of murine and human cells was used as a model for optimization of this approach as reported in biofabrication literature, showing the capability to produce a complex *in vitro* 3D model using a supporting bath [52].

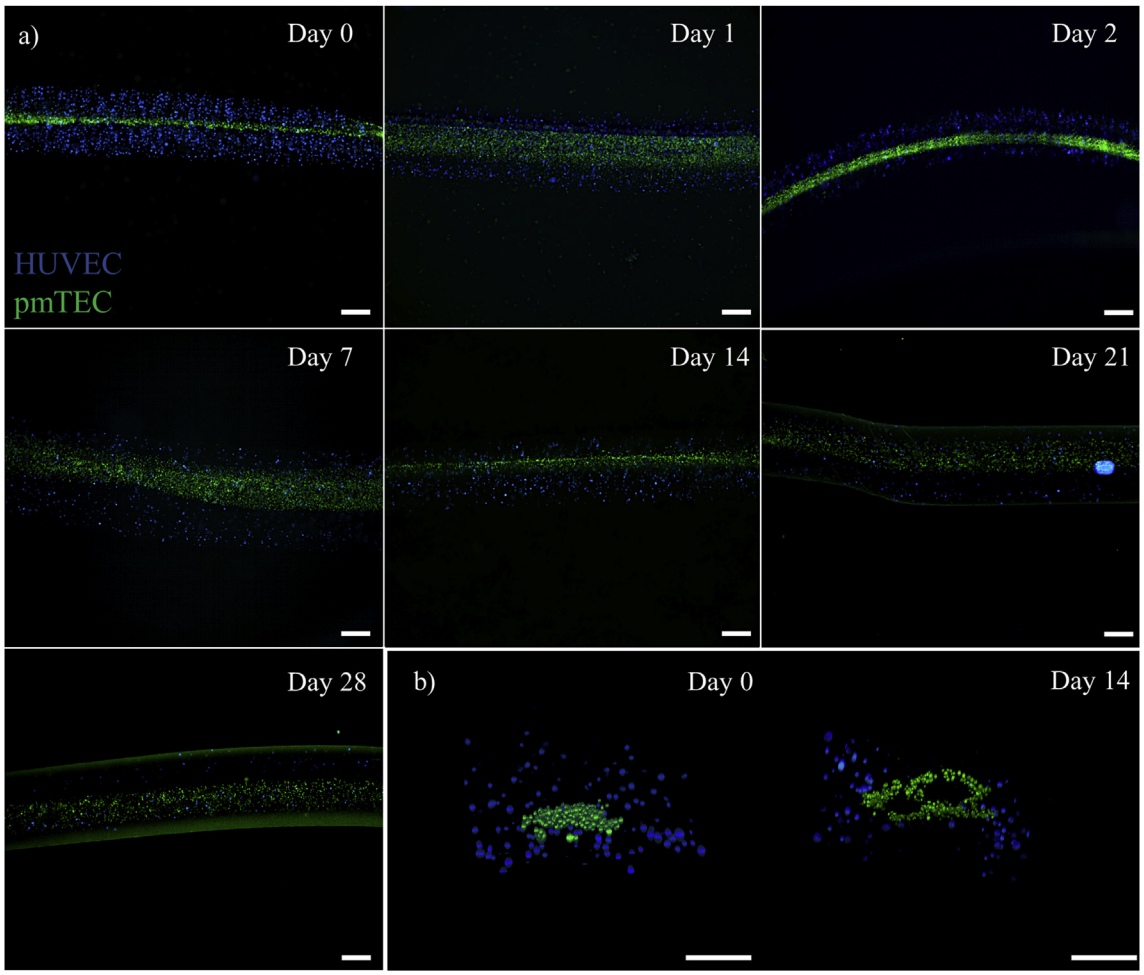

Fig. 6. Core-shell bioprinted filaments made with blue-stained HUVEC as part of the shell and green-stained pmTEC as part of the core. a) Individual samples where imaged on day 0 (after bioprinting), day 1, 2, 7, 14, 21 and 28. Images represent a merged z-stack previously deconvoluted and focused. b) Confocal images of the core-shell filaments showing the formation of the hollow filament during the culture period, from day 0 to day 14. Scale bar = 200 μm.

4. Conclusion

We established a method to efficiently isolate and culture primary tubular epithelial cells and fibroblasts from healthy and diseased murine kidneys. A microfluidic 3D bioprinter was used to manufacture constructs with bioinks of epithelial cells and endothelial cells combined with polysaccharides. A bioprinted core-shell hollow filament, manufactured with pmTECs and HUVECs was manufactured, to build an *in vitro* model. Further steps will be investigated in the future to build on the complexity of the model close to the native structure of the renal tubulointerstitium and with functionality assessment. This preliminary microfluidic bioprinted model could be used in the future to investigate underlying pathomechanisms in renal diseases and the progression of renal fibrosis. Considering the currently limited number of *in vitro* models, our approach might also help to reduce the number of animals required for research.

CRediT authorship contribution statement

Gabriele Addario: Conceptualization, Methodology, Formal analysis, Investigation, Writing - original draft, Writing - review & editing. **Sonja Djudjaj:** Conceptualization, Methodology, Formal analysis, Investigation, Writing - original draft, Writing - review & editing. **Silvia Farè:** Writing - review & editing. **Peter Boor:** Writing - review & editing, Supervision, Resources. **Lorenzo Moroni:** Writing - review & editing, Supervision, Resources. **Carlos Mota:** Conceptualization, Methodology, Formal analysis, Investigation, Writing - original draft, Writing - review & editing, Supervision, Resources.

Declaration of competing interest

The authors declare that they have no known competing financial interests or personal relationships that could have appeared to influence the work reported in this paper.

Acknowledgements

We are grateful to the Dutch Kidney Foundation (Nierstichting Nederland, grant 18OI17 – Innovation Call 2018) and to the funding from the European Union's Horizon 2020 research and innovation programme under the Marie Skłodowska-Curie grant agreement No 860715. We also acknowledge support from the Dutch Province of Limburg. Dr. Matthew Baker and Antonio Feliciano are acknowledge for the HPLC support. This study was financially supported by the German Research Foundation (DFG: SFB/TRR57, SFB/TRR219, BO3755/3-1, BO3755/6-1 to PB and DJ100/1-1 to SD) and the German Ministry of Education and Research (BMBF: STOP-FSGS-01GM1901A) to PB and SD. Carmen. G. Tag (Division of Gastroenterology, RWTH Aachen, Germany) is acknowledge for FACS support.

Appendix

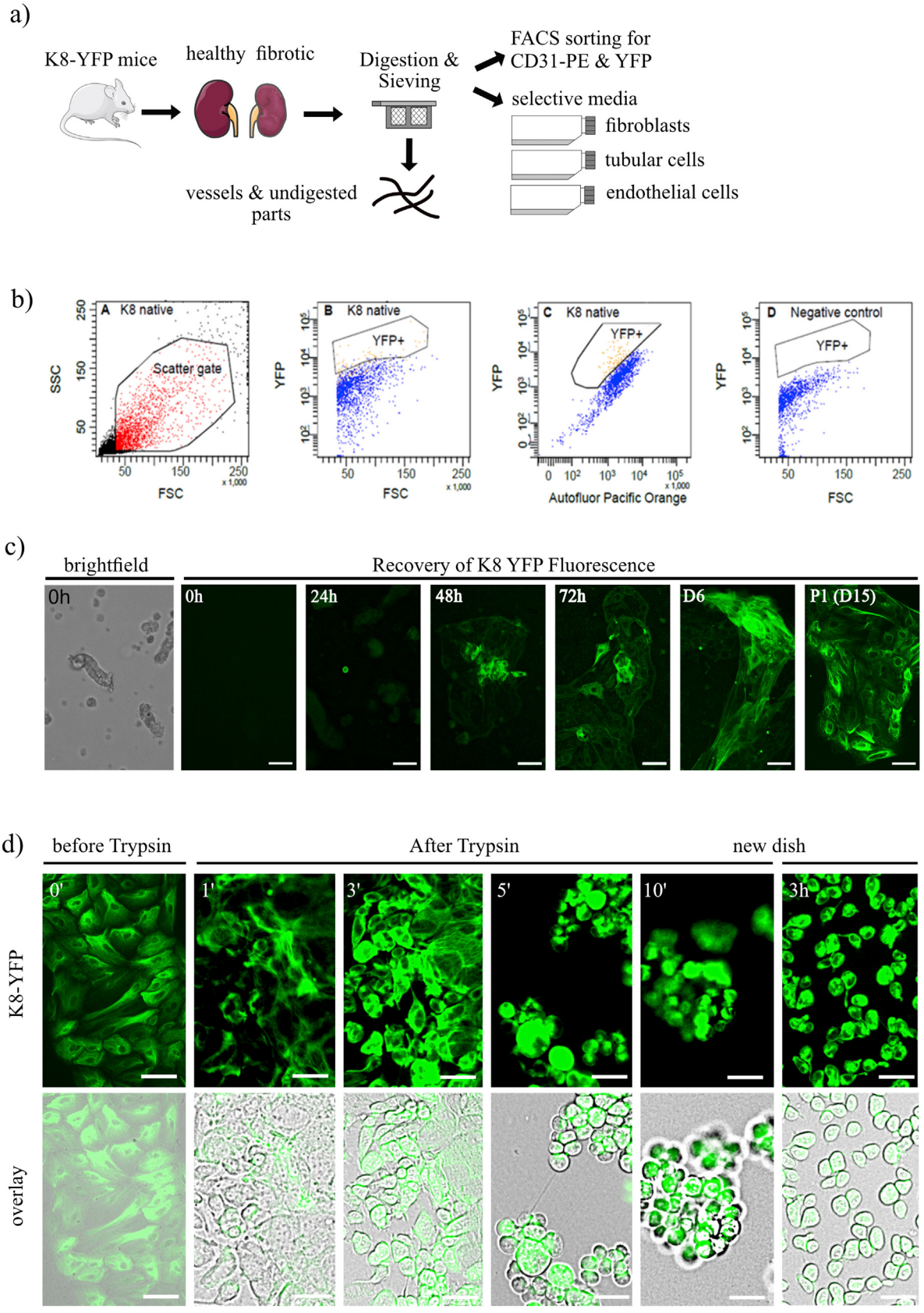

FigS1. Cell isolation and validation. a) Schematic representation of isolation procedure for primary murine tubular epithelial cells (pmTECs), endothelial cells and fibroblasts (pmFibroblasts) from K8-YFP mice. After sieving cells were cultured in selective media or used for FACS sorting. b) FACS analysis of the singe cell suspension for K8-YFP fluorescence for FACS sorting revealed only a weak intensity of the signal and only 5.8% YFP-positive cells were detectable. c) Directly after the

isolation procedure the YFP signal was analysed over a time period of 15 days. Signal was weak directly after isolation, but recovers over the first 24h. Scale bar = 50 μm d) To analyse the signal intensity during cell passing fluorescence analysis of K8-YFP was performed during the trypsinization of the cells over a time period of three hours. Scale bar = 50 μm

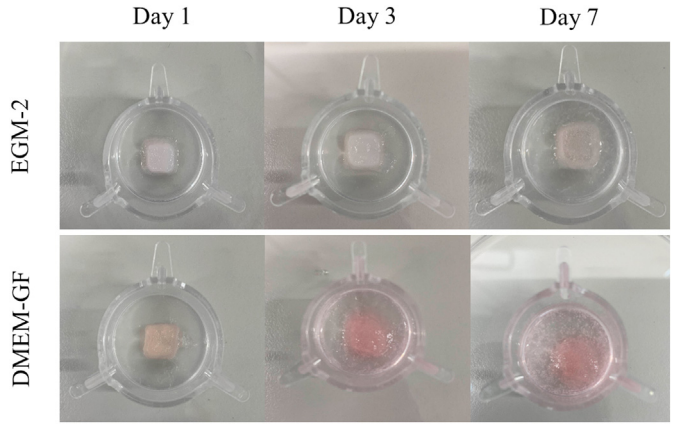

FigS2. Representative brightfield images showing the overall structural stability over the seven day culture for the two culture mediums tested, i.e. EGM-2 and DMEM-GF, where the overall stability increased for the scaffolds cultured with EGM-2. These scaffolds were bioprinted without cells using the IH_alginate solution. The scaffolds were bioprinted in cell culture inserts to preserve the overall structure right after the bioprinting session. Outer top diameter of cell culture insert for 6 well plates: 27.85 mm.

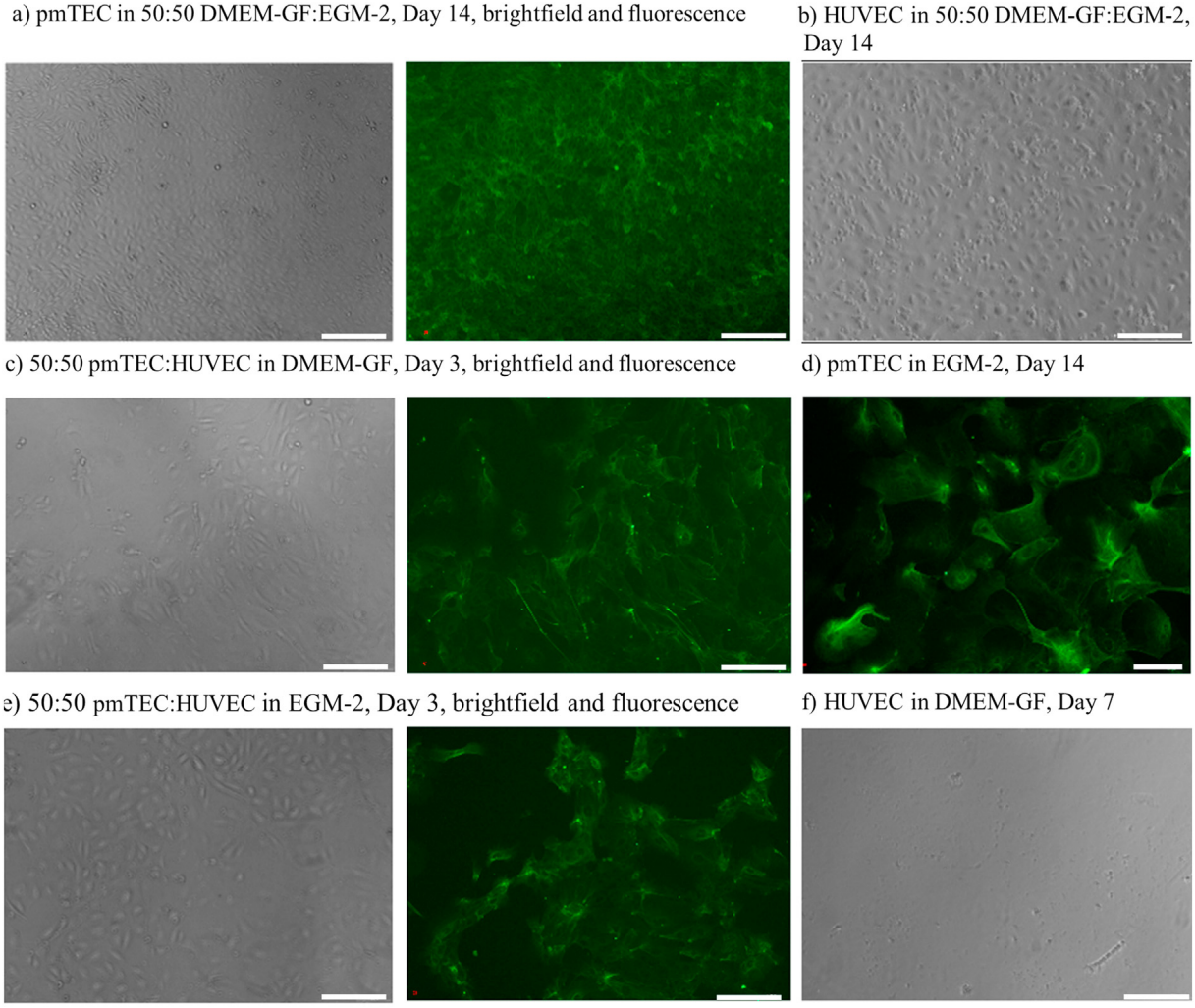

FigS3. Representative morphological analysis showing combinations of pmTEC and HUVEC in the different culture media tested: a) pmTEC in a 50:50 mixture of tubular-specific DMEM-GF and endothelial specific EGM-2 medium, Day 14, brightfield and fluorescence; b) HUVEC in 50:50 mixture of DMEM-GF:EGM-2, Day 14; c) 50:50 mixture pmTEC and HUVEC cells in DMEM-GF, Day 3, brigthfield and fluorescence; d) pmTEC in EGM-2, Day 14; e) 50:50 pmTEC:HUVEC in EGM-2, Day 3, brightfield and fluorescence; f) HUVEC in DMEM-GF, Day 7. Scale bar = 1 mm.

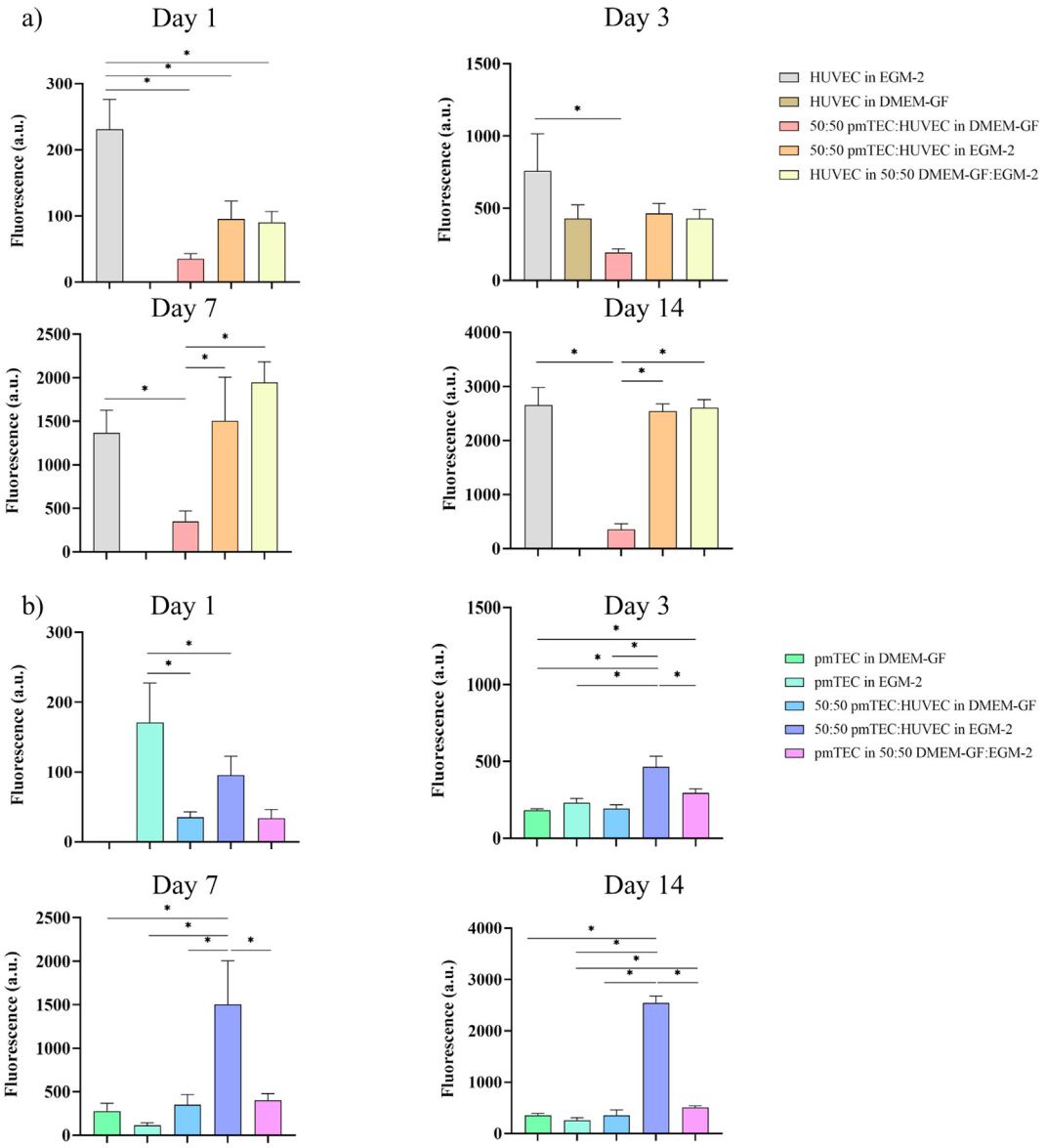

FigS4. Metabolic activity measurements testing different combinations of cells and culture media (Table 1), with a fixed incubation period of 30 min. Measurements were made on day 1, day 3, day 7 and day 14. a) Analysis of the metabolic activity for the culture of HUVEC; b) analysis of the metabolic activity for the culture of pmTEC. Only positive values of fluorescence are plotted. Statistically significant differences (*) for $p<0.05$ are highlighted.

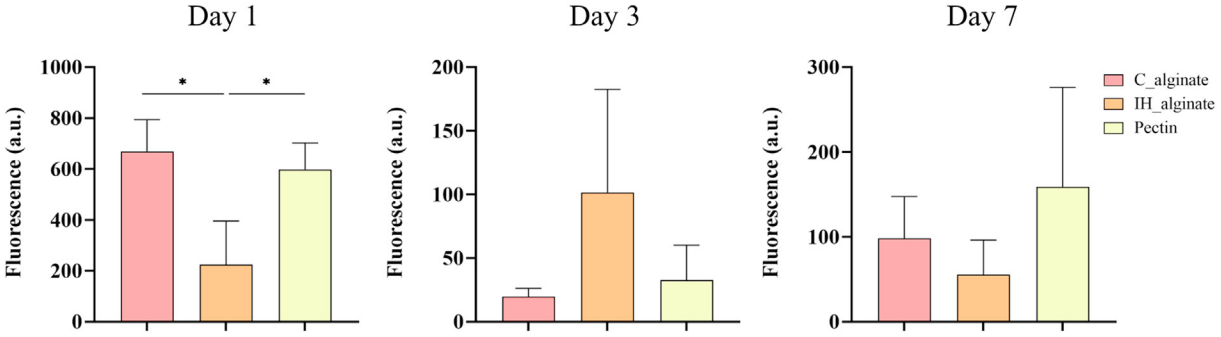

FigS5. Metabolic activity assay of HUVECs encapsulated in commercial alginate (C_alginate), in-house alginate (IH_alginate), and pectin evaluated on day 1, 3, and 7, at 2 hours, in three independent experiments for each timepoint. Statistically significant difference (*) for $p<0.05$.

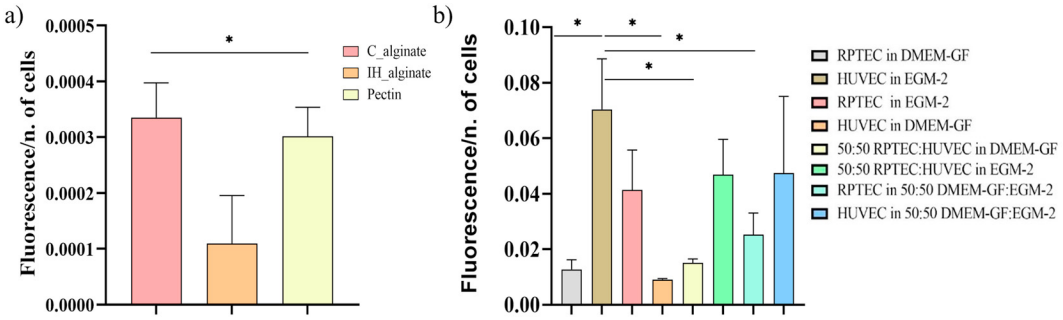

FigS6. Metabolic activity assay of HUVECs in EGM-2 measured on day 1, after 2 hours of incubation of resazurin. Data presented as the measured fluorescence divided by the number of cells. a) HUVECs encapsulated in droplets of commercial alginate (C_alginate), in-house alginate (IH_alginate) and pectin; b) monolayers of cells for the different combinations of cells and media tested (Table 1). Statistically significant difference (*) for $p<0.05$.

References

[1] K. Jansen, C.C.L. Schuurmans, J. Jansen, R. Masereeuw, T. Vermonden, Hydrogel-based cell therapies for kidney regeneration: current trends in biofabrication and in vivo repair, Curr. Pharmaceut. Des. 23 (26) (2017), https://doi.org/10.2174/1381612823666170710155726.

[2] J.S. Uzarski, Y. Xia, J.C. Belmonte, J.A. Wertheim, New strategies in kidney regeneration and tissue engineering, Curr. Opin. Nephrol. Hypertens. 23 (4) (2014) 399–405, https://doi.org/10.1097/01.mnh.0000447019.66970.ea.

[3] N.M. Wragg, L. Burke, S.L. Wilson, A critical review of current progress in 3D kidney biomanufacturing: advances, challenges, and recommendations, Renal Replacement Therapy 5 (1) (2019), https://doi.org/10.1186/s41100-019-0218-7.

[4] E.M. Buhl, S. Djudjaj, B.M. Klinkhammer, K. Ermert, V.G. Puelles, M.T. Lindenmeyer, C.D. Cohen, C. He, E. Borkham-Kamphorst, R. Weiskirchen, B. Denecke, P. Trairatphisan, J. Saez-Rodriguez, T.B. Huber, L.E. Olson, J. Floege, P. Boor, Dysregulated mesenchymal PDGFR-beta drives kidney fibrosis, EMBO Mol. Med. 12 (3) (2020), e11021, https://doi.org/10.15252/emmm.201911021.

[5] J. Majo, B.M. Klinkhammer, P. Boor, D. Tiniakos, Pathology and natural history of organ fibrosis, Curr. Opin. Pharmacol. 49 (2019) 82–89, https://doi.org/10.1016/j.coph.2019.09.009.

[6] S. Djudjaj, P. Boor, Cellular and molecular mechanisms of kidney fibrosis, Mol. Aspect. Med. 65 (2019) 16–36, https://doi.org/10.1016/j.mam.2018.06.002.

[7] Y. Sato, M. Yanagita, Resident fibroblasts in the kidney: a major driver of fibrosis and inflammation, Inflamm. Regen. 37 (2017) 17, https://doi.org/10.1186/s41232-017-0048-3.

[8] Y. Liu, Epithelial to mesenchymal transition in renal fibrogenesis: pathologic significance, molecular mechanism, and therapeutic intervention, J. Am. Soc. Nephrol. 15 (1) (2004) 1–12, https://doi.org/10.1097/01.asn.0000106015.29070.e7.

[9] B.D. Humphreys, S.L. Lin, A. Kobayashi, T.E. Hudson, B.T. Nowlin, J.V. Bonventre, M.T. Valerius, A.P. McMahon, J.S. Duffield, Fate tracing reveals the pericyte and not epithelial origin of myofibroblasts in kidney fibrosis, Am. J. Pathol. 176 (1) (2010) 85–97, https://doi.org/10.2353/ajpath.2010.090517.

[10] T.M. Desrochers, E. Palma, D.L. Kaplan, Tissue-engineered kidney disease models, Adv. Drug Deliv. Rev. 69–70 (2014) 67–80, https://doi.org/10.1016/j.addr.2013.12.002.

[11] N.Y.C. Lin, K.A. Homan, S.S. Robinson, D.B. Kolesky, N. Duarte, A. Moisan, J.A. Lewis, Renal reabsorption in 3D vascularized proximal tubule models, Proc. Natl. Acad. Sci. U. S. A. 116 (12) (2019) 5399–5404, https://doi.org/10.1073/pnas.1815208116.

[12] S. Moll, M. Ebeling, F. Weibel, A. Farina, A. Araujo Del Rosario, J.C. Hoflack, S. Pomposiello, M. Prunotto, Epithelial cells as active player in fibrosis: findings from an in vitro model, PLoS One 8 (2) (2013), e56575, https://doi.org/10.1371/journal.pone.0056575.

[13] C. Mota, S. Camarero-Espinosa, M.B. Baker, P. Wieringa, L. Moroni, Bioprinting: from tissue and organ development to in vitro models, Chem. Rev. (2020), https://doi.org/10.1021/acs.chemrev.9b00789.

[14] K.A. Homan, D.B. Kolesky, M.A. Skylar-Scott, J. Herrmann, H. Obuobi, A. Moisan, J.A. Lewis, Bioprinting of 3D convoluted renal proximal tubules on perfusable chips, Sci. Rep. 6 (2016) 34845, https://doi.org/10.1038/srep34845.

[15] D.B. Kolesky, K.A. Homan, M.A. Skylar-Scott, J.A. Lewis, Three-dimensional bioprinting of thick vascularized tissues, Proc. Natl. Acad. Sci. Unit. States Am. 113 (12) (2016) 3179–3184, https://doi.org/10.1073/pnas.1521342113.

[16] N.K. Singh, W. Han, S.A. Nam, J.W. Kim, J.Y. Kim, Y.K. Kim, D.W. Cho, Three-dimensional cell-printing of advanced renal tubular tissue analogue, Biomaterials 232 (2020) 119734, https://doi.org/10.1016/j.biomaterials.2019.119734.

[17] C.R.C. van Roeyen, F.G. Scurt, S. Brandt, V.A. Kuhl, S. Martinkus, S. Djudjaj, U. Raffetseder, H.-D. Royer, I. Stefanidis, S.E. Dunn, S. Dooley, H. Weng, T. Fischer, J.A. Lindquist, P.R. Mertens, Cold shock Y-box protein-1 proteolysis autoregulates its transcriptional activities, Cell Commun. Signal. : CCS 11 (2013), https://doi.org/10.1186/1478-811X-11-63, 63-63.

[18] S.C. Neves, D.B. Gomes, A. Sousa, S.J. Bidarra, P. Petrini, L. Moroni, C.C. Barrias, P.L. Granja, Biofunctionalized pectin hydrogels as 3D cellular microenvironments, J. Mater. Chem. B 3 (10) (2015) 2096–2108, https://doi.org/10.1039/c4tb00885e.

[19] S.M. Krall, R.F. McFeeters, Pectin hydrolysis: effect of temperature, degree of methylation, pH, and calcium on hydrolysis rates, J. Agric. Food Chem. 6 (4) (1998) 1311–1315.

[20] H.L.H.S. Owens, R.C. Merrill, M. Peterson, Viscosities of Pectin Solutions, vol. 66, 1944.

[21] J. Surh, E. Decker, D. McClements, Influence of pH and pectin type on properties and stability of sodium-caseinate stabilized oil-in-water emulsions, Food Hydrocolloids 20 (5) (2006) 607–618, https://doi.org/10.1016/j.foodhyd.2005.07.004.

[22] K. Itoh, T. Hirayama, A. Takahashi, W. Kubo, S. Miyazaki, M. Dairaku, M. Togashi, R. Mikami, D. Attwood, In situ gelling pectin formulations for oral drug delivery at high gastric pH, Int. J. Pharm. 335 (1–2) (2007) 90–96, https://doi.org/10.1016/j.ijpharm.2006.10.042.

[23] M.C. Coelho Júnior, Guilherme C. Guimarães, Edwin E. Garcia Rojas, Density and kinematic viscosity of pectin aqueous solution, J. Chem. Eng. (54) (2009) 662–667.

[24] J.R. Lorsch, F.S. Collins, J. Lippincott-Schwartz, Fixing problems with cell lines, Science 346 (2014) 1452–1453.

[25] C. Pan, C. Kumar, S. Bohl, U. Klingmueller, M. Mann, Comparative proteomic phenotyping of cell lines and primary cells to assess preservation of cell type-specific functions, Mol. Cell. Proteomics 8 (3) (2009) 443–450, https://doi.org/10.1074/mcp.M800258-MCP200.

[26] N. Schwarz, R. Windoffer, T.M. Magin, R.E. Leube, Dissection of keratin network formation, turnover and reorganization in living murine embryos, Sci. Rep. 5 (2015) 9007, https://doi.org/10.1038/srep09007.

[27] S. Djudjaj, M. Papasotiriou, R.D. Bulow, A. Wagnerova, M.T. Lindenmeyer, C.D. Cohen, P. Strnad, D.S. Goumenos, J. Floege, P. Boor, Keratins are novel markers of renal epithelial cell injury, Kidney Int. 89 (4) (2016) 792–808, https://doi.org/10.1016/j.kint.2015.10.015.

[28] Y. Qin, Seaweed hydrocolloids as thickening, gelling, and emulsifying agents in functional food products, in: Y. Qin (Ed.), Bioactive Seaweeds for Food Applications, Academic Press, 2018, pp. 135–152.

[29] A. Forget, A. Blaeser, F. Miessmer, M. Kopf, D.F.D. Campos, N.H. Voelcker, A. Blencowe, H. Fischer, V.P. Shastri, Mechanically tunable bioink for 3D bioprinting of human cells, Adv Healthc Mater 6 (20) (2017), https://doi.org/10.1002/adhm.201700255.

[30] O. Yuliarti, A.L.S. Hoon, S.Y. Chong, Influence of pH, pectin and Ca concentration on gelation properties of low-methoxyl pectin extracted from Cyclea barbata Miers, Food Struct. 11 (2017) 16–23, https://doi.org/10.1016/j.foostr.2016.10.005.

[31] M. Costantini, S. Testa, P. Mozetic, A. Barbetta, C. Fuoco, E. Fornetti, F. Tamiro, S. Bernardini, J. Jaroszewicz, W. Swieszkowski, M. Trombetta, L. Castagnoli, D. Seliktar, P. Garstecki, G. Cesareni, S. Cannata, A. Rainer, C. Gargioli, Microfluidic-enhanced 3D bioprinting of aligned myoblast-laden hydrogels leads to functionally organized myofibers in vitro and in vivo, Biomaterials 131 (2017) 98–110, https://doi.org/10.1016/j.biomaterials.2017.03.026.

[32] J. Idaszek, M. Costantini, T.A. Karlsen, J. Jaroszewicz, C. Colosi, S. Testa, E. Fornetti, S. Bernardini, M. Seta, K. Kasarello, R. Wrzesien, S. Cannata, A. Barbetta, C. Gargioli, J.E. Brinchman, W. Swieszkowski, 3D bioprinting of hydrogel constructs with cell and material gradients for the regeneration of full-thickness chondral defect using a microfluidic printing head, Biofabrication 11 (4) (2019), 044101, https://doi.org/10.1088/1758-5090/ab2622.

[33] Y.S. Zhang, R. Oklu, M.R. Dokmeci, A. Khademhosseini, Three-Dimensional bioprinting strategies for tissue engineering, Cold Spring Harb Perspect Med 8 (2) (2018), https://doi.org/10.1101/cshperspect.a025718.

[34] Q. Pi, S. Maharjan, X. Yan, X. Liu, B. Singh, A.M. van Genderen, F. Robledo-Padilla, R. Parra-Saldivar, N. Hu, W. Jia, C. Xu, J. Kang, S. Hassan, H. Cheng, X. Hou, A. Khademhosseini, Y.S. Zhang, Digitally tunable microfluidic bioprinting of multilayered cannular tissues, Adv. Mater. 30 (43) (2018), e1706913, https://doi.org/10.1002/adma.201706913.

[35] F. Maiullari, M. Costantini, M. Milan, V. Pace, M. Chirivì, S. Maiullari, A. Rainer, D. Baci, H.E.-S. Marei, D. Seliktar, C. Gargioli, C. Bearzi, R. Rizzi, A multi-cellular 3D bioprinting approach for vascularized heart tissue engineering based on HUVECs and iPSC-derived cardiomyocytes, Sci. Rep. 8 (1) (2018), https://doi.org/10.1038/s41598-018-31848-x.

[36] C. Colosi, S.R. Shin, V. Manoharan, S. Massa, M. Costantini, A. Barbetta, M.R. Dokmeci, M. Dentini, A. Khademhosseini, Microfluidic bioprinting of heterogeneous 3D tissue constructs using low-viscosity bioink, Adv. Mater. 28 (4) (2016) 677–684, https://doi.org/10.1002/adma.201503310.

[37] I.T. Ozbolat, Bioprinting scale-up tissue and organ constructs for transplantation, Trends Biotechnol. 33 (7) (2015) 395–400, https://doi.org/10.1016/j.tibtech.2015.04.005.

[38] F. Dolati, Y. Yu, Y. Zhang, A.M. De Jesus, E.A. Sander, I.T. Ozbolat, In vitro evaluation of carbon-nanotube-reinforced bioprintable vascular conduits, Nanotechnology 25 (14) (2014) 145101, https://doi.org/10.1088/0957-4484/25/14/145101.

[39] C.T.D. Dickman, V. Russo, K. Thain, S. Pan, S.T. Beyer, K. Walus, S. Getsios, T. Mohamed, S.J. Wadsworth, Functional characterization of 3D contractile smooth muscle tissues generated using a unique microfluidic 3D bioprinting technology, Faseb. J. 34 (1) (2020) 1652–1664, https://doi.org/10.1096/fj.201901063RR.

[40] J. Hammer, L.H. Han, X. Tong, F. Yang, A facile method to fabricate hydrogels with microchannel-like porosity for tissue engineering, Tissue Eng. C Methods 20 (2) (2014) 169–176, https://doi.org/10.1089/ten.TEC.2013.0176.

[41] F. Kreimendahl, M. Kopf, A.L. Thiebes, D.F. Duarte Campos, A. Blaeser, T. Schmitz-Rode, C. Apel, S. Jockenhoevel, H. Fischer, Three-Dimensional printing and angiogenesis: tailored agarose-type I collagen blends comprise three-dimensional printability and angiogenesis potential for tissue-engineered substitutes, Tissue Eng. C Methods 23 (10) (2017) 604–615, https://doi.org/10.1089/ten.TEC.2017.0234.

[42] S.V. Murphy, A. Atala, 3D bioprinting of tissues and organs, Nat. Biotechnol. 32 (8) (2014) 773–785, https://doi.org/10.1038/nbt.2958.

[43] E. Abelseth, L. Abelseth, L. De la Vega, S.T. Beyer, S.J. Wadsworth, S.M. Willerth, 3D printing of neural tissues derived from human induced pluripotent stem cells using a fibrin-based bioink, ACS Biomater. Sci. Eng. 5 (1) (2018) 234–243, https://doi.org/10.1021/acsbiomaterials.8b01235.

[44] F.E. Freeman, D.J. Kelly, Tuning alginate bioink stiffness and composition for controlled growth factor delivery and to spatially direct MSC fate within bioprinted tissues, Sci. Rep. 7 (1) (2017) 17042, https://doi.org/10.1038/s41598-017-17286-1.

[45] K. Schutz, A.M. Placht, B. Paul, S. Bruggemeier, M. Gelinsky, A. Lode, Three-dimensional plotting of a cell-laden alginate/methylcellulose blend: towards biofabrication of tissue engineering constructs with clinically relevant dimensions, J Tissue Eng Regen Med 11 (5) (2017) 1574–1587, https://doi.org/10.1002/term.2058.

[46] M. Sarker, M. Izadifar, D. Schreyer, X. Chen, Influence of ionic crosslinkers (Ca(2+)/Ba(2+)/Zn(2+)) on the mechanical and biological properties of 3D Bioplotted Hydrogel Scaffolds, J. Biomater. Sci. Polym. Ed. 29 (10) (2018) 1126–1154, https://doi.org/10.1080/09205063.2018.1433420.

[47] Q. Shu, W. Li, H. Li, G. Sun, Vasostatin inhibits VEGF-induced endothelial cell proliferation, tube formation and induces cell apoptosis under oxygen deprivation, Int. J. Mol. Sci. 15 (4) (2014) 6019–6030, https://doi.org/10.3390/ijms15046019.

[48] L. Ouyang, C.B. Highley, W. Sun, J.A. Burdick, A generalizable strategy for the 3D bioprinting of hydrogels from nonviscous photo-crosslinkable inks, Adv. Mater. 29 (8) (2017), https://doi.org/10.1002/adma.201604983.

[49] R. Attalla, C. Ling, P. Selvaganapathy, Fabrication and characterization of gels with integrated channels using 3D printing with microfluidic nozzle for tissue engineering applications, Biomed. Microdevices 18 (1) (2016), https://doi.org/10.1007/s10544-016-0042-6.

[50] Q. Gao, Y. He, J.Z. Fu, A. Liu, L. Ma, Coaxial nozzle-assisted 3D bioprinting with built-in microchannels for nutrients delivery, Biomaterials 61 (2015) 203–215, https://doi.org/10.1016/j.biomaterials.2015.05.031.

[51] E.J. Weber, A. Chapron, B.D. Chapron, J.L. Voellinger, K.A. Lidberg, C.K. Yeung, Z. Wang, Y. Yamaura, D.W. Hailey, T. Neumann, D.D. Shen, K.E. Thummel, K.A. Muczynski, J. Himmelfarb, E.J. Kelly, Development of a microphysiological model of human kidney proximal tubule function, Kidney Int. 90 (3) (2016) 627–637, https://doi.org/10.1016/j.kint.2016.06.011.

[52] N. Noor, A. Shapira, R. Edri, I. Gal, L. Wertheim, T. Dvir, 3D printing of personalized thick and perfusable cardiac patches and hearts, Adv. Sci. 6 (11) (2019) 1900344, https://doi.org/10.1002/advs.201900344.